

Tensor Canonical Correlation Analysis

You-Lin Chen

Department of Statistics, University of Chicago
and

Mladen Kolar and Ruey S. Tsay
University of Chicago, Booth School of Business

June 30, 2022

Abstract

In many applications, such as classification of images or videos, it is of interest to develop a framework for tensor data instead of ad-hoc way of transforming data to vectors due to the computational and under-sampling issues. In this paper, we study canonical correlation analysis by extending the framework of two dimensional analysis (Lee and Choi, 2007) to tensor-valued data. Instead of adopting the iterative algorithm provided in Lee and Choi (2007), we propose an efficient algorithm, called the higher-order power method, which is commonly used in tensor decomposition and more efficient for large-scale setting. Moreover, we carefully examine theoretical properties of our algorithm and establish a local convergence property via the theory of Lojasiewicz’s inequalities. Our results fill a missing, but crucial, part in the literature on tensor data. For practical applications, we further develop (a) an inexact updating scheme which allows us to use the state-of-the-art stochastic gradient descent algorithm, (b) an effective initialization scheme which alleviates the problem of local optimum in non-convex optimization, and (c) an extension for extracting several canonical components. Empirical analyses on challenging data including gene expression, air pollution indexes in Taiwan, and electricity demand in Australia, show the effectiveness and efficiency of the proposed methodology.

Keywords: Canonical correlation analysis, Deflation, Higher-order power method, Non-convex optimization, Lojasiewicz’s inequalities, Tensor decomposition.

1 Introduction

Canonical Correlation Analysis (CCA) is a widely used multivariate statistical method that aims to learn a low dimensional representation from two sets of data by maximizing the correlation of

linear combinations of two sets of data (Hotelling, 1936). The sets of data could be different views (deformation) of images, different measuring on same object or data with labels. CCA has been widely used in many applications, ranging from text and image retrieval (Mroueh et al., 2016) and image clustering (Jin et al., 2015), to various scientific fields (Hardoon et al., 2004). In contrast to principal component analysis (PCA) (Pearson, 1901), which is an unsupervised learning technique for finding low dimensional data representation, CCA benefits from the label information (Sun and Chen, 2007), other views of data, or correlated side information as in multi-view learning (Sun, 2013).

In this paper, we study CCA in the context of matrix valued and tensor valued data. Matrix valued data has been studied in (Gupta and Nagar, 2000; Kollo and von Rosen, 2005; Werner et al., 2008; Leng and Tang, 2012; Yin and Li, 2012; Zhao and Leng, 2014; Zhou and Li, 2014), while tensor valued data in (Ohlson et al., 2013; Manceur and Dutilleul, 2013; Lu et al., 2011). Practitioners often apply CCA to such data by first converting them into vectors thus destroying the inherent structure present in the samples, increasing the dimensionality of the problem, and increasing the computational complexity. Lee and Choi (2007) proposed a two-dimensional CCA (2DCCA) to address these problems for matrix valued data by preserving data representation and alleviating expensive computation that arises by vectorizing the data. But convergence properties of the iterative singular value decomposition (SVD) algorithm proposed in Lee and Choi (2007) are not known.

In this paper, we develop a power method that can solve the 2DCCA problem faster and provably converges to a stationary point of the objective function. More generally, we present a natural extension of 2DCCA to tensor-valued data that projects the data onto the space of low-rank tensors to maximize the correlation. We present two algorithms for solving the resulting optimization problem, the higher-order power method (HOPM) and, its variant, alternative least squares (ALS), which are particularly effective in a large data setting. HOPM is a widely used algorithm for tensor decomposition (Kolda and Bader, 2009; De Lathauwer et al., 2000a,b), with convergence properties intensely studied in recent years (Wen et al., 2012; Uschmajew, 2015; Xu and Yin, 2013; Li et al., 2015; Guan et al., 2018). However, due to the constraints of the CCA optimization problem, these convergence results are not directly applicable. In order to establish convergence of HOMP for the tensor valued CCA problem, we first establish the equivalence of

HOMP and ALS algorithms. Utilizing this equivalence, we present a transparent convergence proof for the rank one case by applying the theory of analytical gradient flows and Lojasiewicz gradient inequality. The convergence is established in a model-free setting and it applies to any stationary point. We propose an effective initialization procedure to reduce the probability of algorithms getting trapped in a local maximum. Moreover, we develop an inexact updating rule, which enables us to use a gradient descent method suitable for large-scale data and convenient for error analysis. We also discuss how to extend the HOPM for extracting multiple canonical components.

1.1 Main Contributions

We make several contributions in this paper.

First, we interpret 2DCCA (Lee and Choi, 2007) as a non-convex method for the low rank tensor factorization problem. This allows us to formulate a novel tensor extension of 2DCCA, which we term tensor canonical correlation analysis (TCCA). Kim et al. (2007) and Luo et al. (2015) discuss tensor extension of CCA in different settings. The former stresses correlation between each mode, while the latter discusses CCA when multiple views of data are available. None of them provide theoretical justifications or efficient algorithms. See Section 1.2 for more discussions.

Second, we develop the higher-order power method and, its variant, alternating least squares for solving the TCCA problem. One obstacle in analysis of tensor factorization is unidentifiability, that is, if $U_1 \circ U_2$ is a solution, then $U_1/c \circ cU_2$ is also a solution. Thus, without additional regularization or penalty, there is no guarantee to prevent the iteration sequence of the HOPM from going to 0 or infinity. Moreover, this property also implies that it is possible for the iteration sequence to oscillate even when the sequence is close to a stationary point. We illustrate this in Section 6. In other words, the local convergence may not hold for the HOPM. To circumvent this difficulty and seek further numerical stability, we propose the ALS, which uses a different normalization scheme, and show that HOPM and ALS with the same initialization are equivalent. See Proposition 3 for a formal statement. Utilizing this insight and borrowing tools from tensor factorization, we show that ALS and, hence, HOPM have the local convergence property.

Third, we consider several practical issues that arise in analysis of real data. We provide an

effective initialization scheme to reduce the probability of the algorithm getting trapped in a poor local optimum and develop a faster algorithm for large scale data. Furthermore, we discuss the TCCA generalization to (k_1, \dots, k_m) -TCCA, which allows for extraction of multiple features from data. We justify the generalization under a probabilistic model. A deflation procedure is provided for practical applications.

Finally, we apply our method to several real data sets, including gene expression data, air pollution data, and electricity demands. The results demonstrate that our method is efficient and effective even in the extremely high-dimensional setting and can be used to extract useful and interpretable features from the data.

1.2 Related Work

Two papers in the literature are closely related to our tensor canonical correlation analysis. [Luo et al. \(2015\)](#) consider multiple-view extension of CCA, which results in a tensor covariance structure. However, they only consider the vector-valued data, so the vectorization is still required in their setting. [Kim et al. \(2007\)](#) extend CCA to the tensor data, focusing on 3 dimensional videos, but only consider joint space-time linear relationships, which is neither the low-rank approximation of CCA nor the extension of 2DCCA. Moreover, none of the aforementioned papers provide convergence analysis or efficient algorithms, as we detail in Section 4. Furthermore, 2DCCA ([Lee and Choi, 2007](#)) and other 2D extensions proposed in the literature ([Yang et al., 2004](#); [Ye et al., 2004](#); [Zhang and Zhou, 2005](#); [Yang et al., 2008](#)) also lack rigorous analysis.

Various extensions of CCA are available in the literature. Kernel method aims to extract nonlinear relations via implicitly mapping data to a high-dimensional feature space ([Hardoon et al., 2004](#); [Fukumizu et al., 2007](#)). Other nonlinear transformations have been considered to extract more sophisticated relations embedded in the data. [Andrew et al. \(2013\)](#) utilized neural networks to learn nonlinear transformations, [Michaeli et al. \(2016\)](#) used Lancaster’s theory to extend CCA to a nonparametric setting, while [Lopez-Paz et al. \(2014\)](#) proposed a randomized nonlinear CCA, which uses random features to approximate a kernel matrix. [Bach and Jordan \(2006\)](#) and [Safayani et al. \(2018\)](#) interpreted CCA as a latent variable model, which allows development of an EM algorithm for parameter estimation. In the probabilistic setting, [Wang et al. \(2016b\)](#) developed variational inference. In general, nonlinear extensions of CCA often lead to complicated

optimization problems and lack rigorous theoretical justifications.

Our work is also related to scalable methods for solving the CCA problem. Although CCA can be solved as a generalized eigenvalue problem,¹ computing singular value (or eigenvalue) decomposition of a large (covariance) matrix is computationally expensive. Finding an efficient optimization method for CCA remains an important problem, especially for large-scale data, and has been intensively studied (Yger et al., 2012; Ge et al., 2016; Allen-Zhu and Li, 2017; Xu et al., 2018; Fu et al., 2017; Arora et al., 2017; Bhatia et al., 2018). Ma et al. (2015) and Wang et al. (2016a) are particularly related to our work. Wang et al. (2016a) formulated CCA as a regularized least squares problem and solved it with a stochastic gradient descent. Inspired by their work, we optimize the TCCA objective using an alternating least squares algorithm and bound its error accumulation in Section 5. Ma et al. (2015) developed an augmented approximate gradient (AppGrad) scheme to avoid computing the inverse of a large matrix. Although AppGrad does not directly maximize the correlation in each iteration, it can be shown that the CCA solution is a fixed point of the AppGrad scheme. Therefore, if the initialization is sufficiently close to the global CCA solution, the iterates of AppGrad would converge to it. A similar observation holds for the HOPM and ALS algorithms developed in this paper, with the difference that we use the alternating minimization instead of gradient descent. More details and discussions are provided in Section 4.2

1.3 Organization of the paper

In Section 2, we define basic notation and operators of multilinear algebra and introduce the Lojasiewicz inequality. Section 3 reviews the concept of CCA as well as 2DCCA and formulates the tensor CCA. Section 4 presents our algorithms, HOPM and ALS, and studies their convergence. Section 5 deals with practical considerations including an inexact updating rule, effective initialization, and extension to higher rank tensors. Numerical simulations verifying the theoretical results and applications to real data are given in Section 6. All technical proofs can be found in the appendix.

¹See Section 3.1 for details.

2 Preliminaries

In this section, we provide necessary background for the subsequent analysis. First, we present some basic notation and operators in multilinear algebra. Then, we introduce the Lojasiewicz inequality and the associated convergence results.

2.1 Multilinear Algebra and Notation

We briefly introduce notation and concepts in multilinear algebra needed for our analysis. See [Kolda and Bader \(2009\)](#) for more details. We start by introducing the notion of multi-dimensional arrays, which are called tensors. The order of a tensor, also called way or mode, is the number of dimensions the tensor has. For example, a vector is a first-order tensor, and a matrix is a second-order tensor. We use the following convention to distinguish between scalars, vectors, matrices, and higher-order tensors: scalars are denoted by lower-case letters ($a, b, c, \dots; \alpha, \beta, \gamma, \dots$), vectors by upper-case letters (A, B, \dots, X, Y), matrices by bold-face upper-case letters ($\mathbf{A}, \mathbf{B}, \dots, \mathbf{X}, \mathbf{Y}$), and tensors by calligraphic letters ($\mathcal{A}, \mathcal{B}, \dots, \mathcal{X}, \mathcal{Y}$). For an m -mode tensor $\mathcal{X} \in \mathbb{R}^{d_1 \times \dots \times d_m}$, we let its (i_1, \dots, i_m) -th element be $x_{i_1 i_2 \dots i_m}$ or $(\mathcal{X})_{i_1 i_2 \dots i_m}$.

Next, we define some useful operators in multilinear algebra. Matricization, also known as unfolding, is a process of transforming a tensor into a matrix. The mode- a matricization of a tensor \mathcal{X} is denoted by $\mathcal{X}_{(a)}$ and arranges the mode- a fibers to be the columns of the resulting matrix. More specifically, tensor element (i_1, \dots, i_m) maps to matrix element (i_a, j) , where $j = 1 + \sum_{k=1, k \neq a}^m (i_k - 1)j_k$ with $j_k = \prod_{q=1, q \neq a}^{k-1} i_q$. The vector obtained by vectorization of \mathcal{X} is denoted by $\text{vec}(\mathcal{X})$. The Frobenius norm of the tensor \mathcal{X} is defined as $\|\mathcal{X}\|_F^2 = \langle \mathcal{X}, \mathcal{X} \rangle$, where $\langle \cdot, \cdot \rangle$ is the inner product defined on two tensors $\mathcal{X} \in \mathbb{R}^{d_1 \times \dots \times d_m}$, $\mathcal{Y} \in \mathbb{R}^{d_1 \times \dots \times d_m}$ and given by

$$\langle \mathcal{X}, \mathcal{Y} \rangle = \sum_{i_1=1}^{d_1} \dots \sum_{i_m=1}^{d_m} x_{i_1 i_2 \dots i_m} y_{i_1 i_2 \dots i_m}.$$

The mode- k product of a tensor $\mathcal{X} \in \mathbb{R}^{d_1 \times \dots \times d_m}$ with a matrix $\mathbf{A} \in \mathbb{R}^{a \times d_k}$ is a tensor of size $d_1 \times \dots \times d_{k-1} \times a \times d_{k+1} \times \dots \times d_m$ defined by

$$(\mathcal{X} \times_k \mathbf{A})_{i_1 \dots i_{n-1} j i_{n+1} \dots i_m} = \sum_{i_k=1}^{d_k} x_{i_1 i_2 \dots i_m} a_{j i_k}.$$

The outer product of vectors $U_1 \in \mathbb{R}^{d_1}, \dots, U_m \in \mathbb{R}^{d_m}$ is an m -order tensor defined by

$$(U_1 \circ \dots \circ U_m)_{i_1 i_2 \dots i_m} = (U_1)_{i_1} \dots (U_m)_{i_m}.$$

The Kronecker product of two matrices $\mathbf{A} \in \mathbb{R}^{m \times n}$ and $\mathbf{B} \in \mathbb{R}^{p \times q}$ is an $mp \times nq$ matrix given by $\mathbf{A} \otimes \mathbf{B} = (a_{ij} \mathbf{B})_{mp \times nq}$. We call \mathcal{X} a rank-one tensor if there exist vectors X_1, \dots, X_d such that $\mathcal{X} = X_1 \circ \dots \circ X_d$. Given n samples $\{\mathcal{X}_t\}_{t=1}^n$, it is also useful to define the data tensor $\mathcal{X}_{1:n} \in \mathbb{R}^{n \times d_1 \times \dots \times d_m}$ with elements $(\mathcal{X}_{1:n})_{t, j_1, \dots, j_m} = (\mathcal{X}_t)_{j_1, \dots, j_m}$.

2.2 Convergence Analysis via Lojasiewicz Inequality

There are two common approaches for establishing convergence of non-convex methods. One assumes that the initial point and the global optimum lie in a convergence region that is locally convex and, thus, the optimization procedure converges to the global optimum. For certain problems, there are effective initialization schemes that provide, with high probability, an initial point that is close enough (within the convergence region) to the global optimum. We provide an effective initialization scheme in Section 5.3 for our method.

Another approach is based on the theory of analytical gradient flows, which allows establishing convergence of gradient descent based algorithms for difficult problems, such as, non-smooth, non-convex, or manifold optimization. This approach is also useful for problems arising in tensor decomposition where the optimum set is not compact and isolated. For example, in the case of PCA or CCA problems, the optimum set is a low dimensional subspace or manifold. The advantage of this approach is that it can be applied to study convergence to all stationary points, without assuming a model for the data. The drawback of the approach is that the convergence rate on a particular problem depends on the Lojasiewicz exponent in Lemma 1 below, which is hard to explicitly compute. However, Liu et al. (2018) recently showed that the Lojasiewicz exponent at any critical point of the quadratic optimization problem with orthogonality constraint is $1/2$, which leads to linear convergence of gradient descent. Li and Pong (2018) developed various calculus rules to deduce the Lojasiewicz exponent.

The method of Lojasiewicz gradient inequality allows us to study an optimization problem

$$\min_{Z \in \mathbb{R}^p} f(Z), \tag{1}$$

where f may not be convex, and we apply a gradient based algorithm for finding stationary points. The key ingredient for establishing linear or sublinear convergence rate is the following Lojasiewicz gradient inequality ([Lojasiewicz, 1965](#)).

Lemma 1 (Lojasiewicz gradient inequality). *Let f be a real analytic function on a neighborhood of a stationary point X in \mathbb{R}^n . Then, there exist constants $c > 0$ and the Lojasiewicz exponent $\theta \in (0, 1/2]$, such that*

$$|f(Y) - f(X)|^{1-\theta} \leq c \|\nabla f(Y)\|, \quad (\text{L})$$

where Y is in some neighborhood of X .

See [Absil et al. \(2005\)](#) and references therein for the proof and discussion. Since the objective function appearing in the CCA optimization problem is a polynomial, we can use the Lojasiewicz gradient inequality in our convergence analysis. Suppose $\{Z_k\}_k$ is a sequence of iterates produced by a descent algorithm that satisfy the following assumptions:

- **Primary descent condition:** there exists $\sigma > 0$ such that, for a sufficiently large k , it holds that

$$f(Z_k) - f(Z_{k+1}) \geq \sigma \|\nabla f(Z_k)\| \|Z_k - Z_{k+1}\|. \quad (\text{A1})$$

- **Stationary condition:** for a sufficiently large k , it holds that

$$\nabla f(Z_k) = 0 \implies Z_k = Z_{k+1}. \quad (\text{A2})$$

- **Asymptotic small step-size safeguard:** there exists $\kappa > 0$ such that, for a large enough k , it holds that

$$\|Z_{k+1} - Z_k\| \geq \kappa \|\nabla f(Z_k)\|. \quad (\text{A3})$$

Then, we have the following theorem which is the main tool we use in our analysis and its proof can be found in [Schneider and Uschmajew \(2015\)](#).

Theorem 2. *Under the condition of Lemma 1 and assumptions (A1) and (A2), if there exists a cluster point Z^* of the sequence (Z_k) satisfying (L), then Z^* is the limit of the sequence, i.e., $Z_k \rightarrow Z^*$. Furthermore, if (A3) holds, then*

$$\|Z_k - Z^*\| \leq C \begin{cases} e^{-ck} & \text{if } \theta = \frac{1}{2} \text{ for some } c > 0, \\ k^{-\theta} & \text{if } 0 < \theta < \frac{1}{2}, \end{cases}$$

for some $C > 0$. Moreover, $\nabla f(Z_k) \rightarrow 0$.

It is not hard to see that the gradient descent iterates for a strongly convex and smooth function f satisfy conditions (A1)-(A3) and Lojasiewicz gradient inequality. Moreover, if one can show that Lojasiewicz’s inequality holds with $\theta = 1/2$ for the set of stationary points, then linear convergence to stationary points can be established (Liu et al., 2018). In fact, they related Lojasiewicz’s inequality to the following error bound (Luo and Tseng, 1993):

$$\|f(X)\| \geq \mu \|X - X^*\|,$$

where $\mu > 0$ and X^* is in the set of stationary points. Karimi et al. (2016) proved that these two conditions actually imply quadratic growth:

$$f(X) - f(X^*) \geq \frac{\mu'}{2} \|X - X^*\|^2,$$

where $\mu' > 0$. This means that f is strongly convex when X is close to a stationary point. Those local conditions are useful in non-convex and even non-smooth, non-Euclidean setting. See Karimi et al. (2016) and Bolte et al. (2017) for more discussions.

3 Tensor Canonical Correlation Analysis

In this section, we review the canonical correlation analysis for vector-valued data, focusing on finding the first pair of canonical variables. Next, we present the extension of CCA to the matrix-valued data and our proposal for the tensor-valued data. Section 5.2 discusses how to extend the approach for finding multiple canonical variables. Unless otherwise stated, we assume that all random elements in this paper are zero-mean.

3.1 Canonical Correlation Analysis

We review the classical canonical correlation analysis in this section. Consider two multivariate random vectors $X \in \mathbb{R}^{d_x}$ and $Y \in \mathbb{R}^{d_y}$. The canonical correlation analysis aims to maximize the correlation between the projections of two random vectors and can be formulated as the following maximization problem

$$\max_{U \in \mathbb{R}^{d_x}, V \in \mathbb{R}^{d_y}} \text{corr}(U^\top X, V^\top Y) = \max_{U \in \mathbb{R}^{d_x}, V \in \mathbb{R}^{d_y}} \frac{\text{cov}(U^\top X, V^\top Y)}{\sqrt{\text{var}(U^\top X)\text{var}(V^\top Y)}}. \quad (2)$$

The above optimization problem can be written equivalently in the following constrained form

$$\max_{U,V} U^\top \Sigma_{XY} V \quad \text{s.t.} \quad U^\top \Sigma_{XX} U = 1 = V^\top \Sigma_{YY} V,$$

where, under the zero-mean assumption, $\Sigma_{XY} = \mathbf{E}[XY^\top]$, $\Sigma_{XX} = \mathbf{E}[XX^\top]$, and $\Sigma_{YY} = \mathbf{E}[YY^\top]$. Using the standard technique of Lagrangian multipliers, we can obtain U and V by solving the following generalized eigenvalue problem

$$\begin{bmatrix} 0 & \Sigma_{XY} \\ \Sigma_{YX} & 0 \end{bmatrix} \begin{bmatrix} U \\ V \end{bmatrix} = \lambda \begin{bmatrix} \Sigma_{XX} & 0 \\ 0 & \Sigma_{YY} \end{bmatrix} \begin{bmatrix} U \\ V \end{bmatrix}, \quad (3)$$

where $\Sigma_{YX} = \Sigma_{XY}^\top$ and λ is the Lagrangian multiplier. In practice, the data distribution is unknown, but i.i.d. draws from the distribution are available. We can estimate the canonical correlation coefficients by replacing the expectations with sample averages, leading to the empirical version of the optimization problem.

3.2 Two-Dimensional Canonical Correlation Analysis

Lee and Choi (2007) proposed two-dimensional canonical correlation analysis (2DCCA), which extends CCA to matrix-valued data. The naive way of dealing with matrix-valued data is to reshape each data matrix into a vector and then apply CCA. However, this naive preprocessing procedure breaks the structure of the data and introduces several side effects, including increased computational complexity and larger amount of data required for accurate estimation of canonical directions. To overcome this difficulty, 2DCCA maintains the original data representation and performs CCA-style dimension reduction as follows. Given two data matrices \mathbf{X} , \mathbf{Y} , 2DCCA seeks left and right transformations, L_x, R_x, L_y, R_y , that maximize the correlation between $L_x^\top \mathbf{X} R_x$ and $L_y^\top \mathbf{Y} R_y$ and can be formulated as

$$\max_{L_x, R_x, L_y, R_y} \text{Cov}(L_x^\top \mathbf{X} R_x, L_y^\top \mathbf{Y} R_y) \quad \text{s.t.} \quad \text{Var}(L_x^\top \mathbf{X} R_x) = 1 = \text{Var}(L_y^\top \mathbf{Y} R_y). \quad (4)$$

Lee and Choi (2007) developed an iterative SVD-based algorithm for solving the problem above. The idea is that, for fixed R_x and R_y , $\mathbf{X} R_x$ and $\mathbf{Y} R_y$ are random vectors and L_x and L_y can be obtained using any CCA algorithm. Similarly we can switch the roles of variables and fix L_x and L_y . Thus, the algorithm iterates between updating L_x and L_y with R_x and R_y fixed and updating R_x and R_y with L_x and L_y fixed. We call it SVD-based algorithm, since Lee and Choi

(2007) solves CCA using the generalized eigendecomposition in (3). It is well-known that solving SVD of large matrices is computationally and memory intensive (Arora et al., 2012; Wang et al., 2018). Moreover, there is evidence shown in Section 6 that the sequence of iterates obtained by this procedure oscillates even if the iterates are close to the stationary point. See comparison with HOPM in the last paragraph of Section 4.1.

To the best of our knowledge, no clear interpretation why 2DCCA can improve the classification results, how the method is related to data structure, nor rigorous convergence analysis exists for 2DCCA. We address these issues, by first noting that the 2DCCA problem in (4) can be expressed as

$$\max_{\mathbf{U}, \mathbf{V}: \text{rank}(\mathbf{U})=1=\text{rank}(\mathbf{V})} \text{corr}(\text{Tr}(\mathbf{U}^\top \mathbf{X}), \text{Tr}(\mathbf{V}^\top \mathbf{Y})). \quad (5)$$

Therefore, we can treat 2DCCA as the CCA optimization problem with the low-rank restriction on canonical directions and the SVD-based algorithm is a particular non-convex solver for this constrained program. Furthermore, formulating the optimization problem as in (5) allows us to use techniques based on the Burer-Monteiro factorization (Chen and Wainwright, 2015; Park et al., 2018, 2017; Sun and Dai, 2017; Haeffele et al., 2014) and non-convex optimization (Yu et al., 2018; Zhao et al., 2015; Yu et al., 2017; Li et al., 2019; Yu et al., 2019).

3.3 Canonical Correlation Analysis with Tensor-valued Data

We are ready to present the problem of tensor canonical correlation analysis, which is a natural extension of 2DCCA. Consider two zero-mean random tensors $\mathcal{X} \in \mathbb{R}^{d_1 \times \dots \times d_m}$ and $\mathcal{Y} \in \mathbb{R}^{d_1 \times \dots \times d_m}$. Note that, for simplicity in presentation, we assume the two random tensors \mathcal{X} and \mathcal{Y} have the same mode and shape. Note that this assumption is not needed in the analysis or the algorithm. TCCA seeks two rank-one tensors $\mathcal{U} = U_1 \circ \dots \circ U_m \in \mathbb{R}^{d_1 \times \dots \times d_m}$ and $\mathcal{V} = V_1 \circ \dots \circ V_m \in \mathbb{R}^{d_1 \times \dots \times d_m}$ that maximize the correlation between $\langle \mathcal{U}, \mathcal{X} \rangle$ and $\langle \mathcal{V}, \mathcal{Y} \rangle$,

$$\max_{\mathcal{U}, \mathcal{V}} \text{Corr}(\langle \mathcal{U}, \mathcal{X} \rangle, \langle \mathcal{V}, \mathcal{Y} \rangle). \quad (6)$$

Since the population distribution is unknown, by replacing covariance and cross-covariance matrices by their empirical counterparts, we get the empirical counterpart of the optimization problem in (6)

$$\max_{\mathcal{U}, \mathcal{V}} \rho_n(\mathcal{U}, \mathcal{V}),$$

where $\rho_n(\mathcal{U}, \mathcal{V})$ is the sample correlation defined as

$$\rho_n(\mathcal{U}, \mathcal{V}) = \frac{\frac{1}{n} \sum_{t=1}^n \langle \mathcal{U}, \mathcal{X}_t \rangle \langle \mathcal{V}, \mathcal{Y}_t \rangle}{\sqrt{\frac{1}{n} \sum_{t=1}^n \langle \mathcal{U}, \mathcal{X}_t \rangle^2 \cdot \frac{1}{n} \sum_{t=1}^n \langle \mathcal{V}, \mathcal{Y}_t \rangle^2}} \quad (7)$$

and $\{\mathcal{X}_t, \mathcal{Y}_t\}_{t=1}^n$ are the samples from the unknown distributions of \mathcal{X}, \mathcal{Y} . The following empirical version of residual form of the problem (6) will be useful for developing efficient algorithms

$$\min_{\mathcal{U}, \mathcal{V}} \frac{1}{2n} \sum_{t=1}^n (\langle \mathcal{U}, \mathcal{X}_t \rangle - \langle \mathcal{V}, \mathcal{Y}_t \rangle)^2 \quad \text{s.t.} \quad \frac{1}{n} \sum_{t=1}^n \langle \mathcal{U}, \mathcal{X}_t \rangle^2 = 1 = \frac{1}{n} \sum_{t=1}^n \langle \mathcal{V}, \mathcal{Y}_t \rangle^2. \quad (8)$$

This formulation reveals that TCCA is related to tensor decomposition. Furthermore, the sub-problem obtained by fixing all components of \mathcal{U}, \mathcal{V} except for components U_j or V_j is equivalent to the least squares problem. This allows us to use state-of-the-art solvers based on (stochastic) gradient descent that are especially suitable for large-scale data (Wang et al., 2016a) and develop computationally efficient algorithms for CCA with tensor data proposed in Section 5.

4 Algorithms

We present the higher-order power method and its alternating least squares variant for solving the TCCA problem. Furthermore, we establish convergence results. Note that we only discuss the case of rank one factorization and leave the generalization to Section 5.

4.1 Higher-order Power Method

The power method is a practical tool for finding the leading eigenvector of a matrix, which is used in tensor factorization. There are many interpretations for the power method and here we show that it is minimizing a certain Lagrange function.

The Lagrange function associated with the optimization problem in (8) is

$$\mathcal{L}(\mathcal{U}, \mathcal{V}, \lambda, \mu) = \frac{1}{2n} \sum_{t=1}^n (\langle \mathcal{U}, \mathcal{X}_t \rangle - \langle \mathcal{V}, \mathcal{Y}_t \rangle)^2 + \lambda \left(1 - \frac{1}{n} \sum_{t=1}^n \langle \mathcal{U}, \mathcal{X}_t \rangle^2\right) + \mu \left(1 - \frac{1}{n} \sum_{t=1}^n \langle \mathcal{V}, \mathcal{Y}_t \rangle^2\right), \quad (9)$$

where λ and μ are the Lagrange multipliers. Minimizing the above problem in one component U_j of \mathcal{U} , with the other components of \mathcal{U}, \mathcal{V} fixed, leads to a least squares problem. Define the partial contraction \mathbf{X}_j of $\mathcal{X}_{1:n}$ with all component of \mathcal{U} except U_j as

$$\mathbf{X}_j = \mathcal{X}_{1:n} \times_2 U_1^\top \cdots \times_j U_{j-1}^\top \times_{j+2} U_{j+1}^\top \cdots \times_{m+1} U_m^\top.$$

Similar notation is defined for the partial contraction \mathbf{Y}_j of $\mathcal{Y}_{1:n}$. With this notation, we set the gradients $\nabla_{U_j}\mathcal{L}$ and $\nabla_{\lambda}\mathcal{L}$ equal to zero, which yields the following stationary conditions

$$\begin{aligned}\frac{1-2\lambda}{n}\mathbf{X}_j^\top\mathbf{X}_jU_j &= \frac{1}{n}\mathbf{X}_j^\top\mathbf{Y}_jV_j, \\ 1-2\lambda &= U_j^\top\left(\frac{1}{n}\mathbf{X}_j^\top\mathbf{X}_j\right)U_j.\end{aligned}$$

Combining the two equations with similar stationary conditions for V_j , we obtain the following updating rule

$$U_j = \frac{\mathbf{X}_j^\dagger\mathbf{Y}_jV_j}{\sqrt{V_j^\top\mathbf{Y}_j^\top\mathbf{X}_j\mathbf{X}_j^\dagger\mathbf{Y}_jV_j}}, \quad V_j = \frac{\mathbf{Y}_j^\dagger\mathbf{X}_jU_j}{\sqrt{U_j^\top\mathbf{X}_j^\top\mathbf{Y}_j\mathbf{Y}_j^\dagger\mathbf{X}_jU_j}}, \quad (10)$$

where $\mathbf{X}_j^\dagger, \mathbf{Y}_j^\dagger$ are the pseudo inverses of $\mathbf{X}_j, \mathbf{Y}_j$, respectively. The update (10) is in the form of the power method on matrices $\mathbf{X}_j^\dagger\mathbf{Y}_j\mathbf{Y}_j^\dagger\mathbf{X}_j$ and $\mathbf{Y}_j^\dagger\mathbf{X}_j\mathbf{X}_j^\dagger\mathbf{Y}_j$ (Regalia and Kofidis, 2000; Kolda and Bader, 2009). Cyclically updating each component yields the higher-order power method, which is detailed in Algorithm 1. Note that the updating rule is similar to one in Wang et al. (2017). However, when the mode of the tensor $m > 1$, matrices of power method vary in each iteration, which causes obstacles for theoretical analysis.

It is easy to see that updating one component of \mathcal{U} and \mathcal{V} simultaneously results in a SVD-based algorithm. On the other hand, in HOPM we update only one component in an iteration. For exact updating, the SVD-based algorithm requires SVD in each iteration, which may be computational expensive when the data size is large. HOPM only requires solving a least squares problem, which can be done even in a large scale data setting. From the results of Section 6, we see that the two methods have similar convergence behavior. However, the SVD-based algorithm lacks local convergence property due to the unidentifiability, which is also shown in Section 6. In contrast, by connecting HOPM to alternating least squares method introduced in the next section, we show that HOPM enjoys local convergence property without any additional modifications.

4.2 Alternating Least Squares

In a CCA problem, only the projection subspace is identifiable, since the correlation is scale invariant. Same is true in PCA and partial least squares (PLS) problems in both matrix and tensor cases (Arora et al., 2012; Uschmajew, 2015; Gao et al., 2017). Therefore, normalization steps restricting canonical variables on the unit sphere are only important for numerical stability.

Algorithm 1: Higher-order Power Method and Alternating Least Squares

```

1 Input :  $\mathcal{X}_{1:n}, \mathcal{Y}_{1:n} \in \mathbb{R}^{n \times d_1 \times \dots \times d_m}$ ,  $r_x, r_y \geq 0$ ,  $\epsilon > 0$ 
2 while not converged do
3   for  $j = 1, 2, \dots, m$  do
4      $\mathbf{X}_{kj} = \mathcal{X}_{1:n} \times_2 U_{k1}^\top \cdots \times_j U_{k,j-1}^\top \times_{j+2} U_{k-1,j+1}^\top \cdots \times_{m+1} U_{k-1,m}^\top$ 
5      $\mathbf{Y}_{kj} = \mathcal{Y}_{1:n} \times_2 V_{k1}^\top \cdots \times_j V_{k,j-1}^\top \times_{j+2} V_{k-1,j+1}^\top \cdots \times_{m+1} V_{k-1,m}^\top$ 
6     option I (exact updating):  $\tilde{U}_{kj} = (\mathbf{X}_{kj}^\top \mathbf{X}_{kj} + r_x \mathbf{I})^{-1} \mathbf{X}_{kj}^\top \mathbf{Y}_{kj} V_{k-1,j}$ 
7     option II (inexact updating):  $\tilde{U}_{kj}$  is an  $\epsilon$ -suboptimum of
      
$$\min_{\tilde{U}} \frac{1}{2n} \|\mathbf{X}_{kj} \tilde{U} - \mathbf{Y}_{kj} V_{k-1,j}\|^2 + \frac{r_x}{2} \|\tilde{U}\|^2$$

8     option I (HOPM):  $U_{kj} = \tilde{U}_{kj} (\tilde{U}_{kj}^\top (\frac{1}{n} \mathbf{X}_{kj}^\top \mathbf{X}_{kj}) \tilde{U}_{kj})^{-1/2}$ 
9     option II (ALS):  $U_{kj} = \tilde{U}_{kj} \|\tilde{U}_{kj}\|^{-1}$ 
10    option I (exact updating):  $\tilde{V}_{kj} = (\mathbf{Y}_{kj}^\top \mathbf{Y}_{kj} + r_y \mathbf{I})^{-1} \mathbf{Y}_{kj}^\top \mathbf{X}_{kj} U_{kj}$ 
11    option II (inexact updating):  $\tilde{V}_{k-1,j}$  is an  $\epsilon$ -suboptimum of
      
$$\min_{\tilde{V}} \frac{1}{2n} \|\mathbf{X}_{kj} \tilde{U}_{kj} - \mathbf{Y}_{kj} \tilde{V}\|^2 + \frac{r_y}{2} \|\tilde{V}\|^2$$

12    option I (HOPM):  $V_{kj} = \tilde{V}_{kj} (\tilde{V}_{kj}^\top (\frac{1}{n} \mathbf{Y}_{kj}^\top \mathbf{Y}_{kj}) \tilde{V}_{kj})^{-1/2}$ 
13    option II (ALS):  $V_{kj} = \tilde{V}_{kj} \|\tilde{V}_{kj}\|^{-1}$ 
14  end
15   $k = k + 1$ 
end
16 Output:  $\mathcal{U}_k, \mathcal{V}_k$ 

```

The major difference between PCA and CCA is that the normalization steps are essential in HOPM for preventing \mathcal{U} and \mathcal{V} iterates from converging to zero quickly.

The key insight we present in this section is that different regularization schemes actually generate the same sequence of correlation values, which is stated formally in Proposition 3. This insight allows us to develop alternating least squares for solving TCCA, which uses the Euclidean norm as regularization. See Algorithm 1. The Euclidean norm provides the simplest form of regularization and does not depend on the data, which increases the numerical stability and allows for simple theoretical analysis. One of the reasons for numerical instability of HOPM comes from rank deficiency of the covariance matrices $\frac{1}{n} \mathbf{X}_{kj}^\top \mathbf{X}_{kj}$ and $\frac{1}{n} \mathbf{Y}_{kj}^\top \mathbf{Y}_{kj}$, which commonly arises in CCA

due to the low rank structure of the data and undersampling. The numerical stability can be improved by adding a regularization term $r\mathbf{I}$ to the empirical covariance matrix.

Another major benefit of ALS is related to identifiability. Observe that if $\mathcal{U} = U_1 \circ \dots \circ U_m$ and $\mathcal{V} = V_1 \circ \dots \circ V_m$ are a stationary point, then $U_1/c \circ U_2 \circ \dots \circ U_{m-1} \circ cU_m$ and $cV_1 \circ V_2 \circ \dots \circ V_{m-1} \circ V_m/c$ are also a stationary point for any non-zero constant c . In particular, the optimum set is not isolated nor compact. In this case, it is possible that the iteration sequence diverges, even while approaching the stationary set. This is the main difficulty in the analysis of convergence in tensor factorization. Moreover, any component approaching zero or infinity causes numerical instability. One way to overcome the numerical instability is by adding a penalty function to balance magnitude of each component. However, using this approach, one cannot find the exact solution when updating each component and the whole optimization process is slowed down. ALS solves the identifiability by restricting each component to a compact sphere.

Note that projection to the unit sphere is not the projection onto the constraint in (8). Therefore, we need to address the question whether HOPM and ALS generate two different sequences of iterates that have different behaviors. The key question is whether ALS minimizes the TCCA objective function in (8). In what follows, we explain how to derive ALS and answer the above question by introducing a new objective function. Consider the modified loss (potential) function

$$\tilde{\mathcal{L}}(\alpha, \mathcal{U}, \beta, \mathcal{V}, \lambda, \mu) = \frac{1}{2n} \sum_{t=1}^n (\langle \alpha \mathcal{U}, \mathcal{X}_t \rangle - \langle \beta \mathcal{V}, \mathcal{Y}_t \rangle)^2 + \lambda \left(1 - \frac{1}{n} \sum_{t=1}^n \langle \alpha \mathcal{U}, \mathcal{X}_t \rangle^2\right) + \mu \left(1 - \frac{1}{n} \sum_{t=1}^n \langle \beta \mathcal{V}, \mathcal{Y}_t \rangle^2\right), \quad (11)$$

where we have added two extra normalization variables to the components of \mathcal{U} and \mathcal{V} . This type of potential function appears in the literature on PCA and tensor decomposition. For example, the following two optimization problems are equivalent for the problem of finding the best rank-one tensor $\mathcal{U} = U_1 \circ U_2 \circ \dots \circ U_m$ approximation of \mathcal{X}

$$\min_{\mathcal{U}, \alpha: \|U_1\| = \dots = \|U_m\| = 1} \|\mathcal{X} - \alpha \mathcal{U}\|^2 \iff \min_{\mathcal{U}} \|\mathcal{X} - \mathcal{U}\|^2.$$

HOPM represents the latter problem which is convex with respect to each component U_j , and the ALS represents the former optimization problem is no longer a convex problem with respect to α and U_j . In the first formula, it is obvious that once \mathcal{U} is found, then so is λ . Therefore, we may ignore α in the optimization procedure, but considering this form is convenient for the analysis.

To see how the ALS relates to (11), given the gradient of the potential

$$\begin{aligned}
\nabla_{U_j} \tilde{\mathcal{L}} &= \frac{\alpha^2(1-2\lambda)}{n} \mathbf{X}_j^\top \mathbf{X}_j U_j - \frac{\alpha\beta}{n} \mathbf{X}_j^\top \mathbf{Y}_j V_j, \\
\nabla_{\alpha} \tilde{\mathcal{L}} &= \frac{\alpha(1-2\lambda)}{n} U_j^\top \mathbf{X}_j^\top \mathbf{X}_j U_j - \frac{\beta}{n} U_j^\top \mathbf{X}_j^\top \mathbf{Y}_j V_j, \\
\nabla_{\lambda} \tilde{\mathcal{L}} &= 1 - \frac{\alpha^2}{n} U_j^\top \mathbf{X}_j^\top \mathbf{X}_j U_j,
\end{aligned} \tag{12}$$

and, similarly for $\nabla_{\beta, V_j, \mu} \tilde{\mathcal{L}}$, and the dynamical iterates of ALS as following

$$\begin{aligned}
U_{kj} &= \mathbf{X}_{kj}^\dagger \mathbf{Y}_{kj} V_{k-1,j} / \|\mathbf{X}_{kj}^\dagger \mathbf{Y}_{kj} V_{k-1,j}\|, \\
\alpha_{kj} &= (U_{k,j}^\top \mathbf{X}_{kj}^\top \mathbf{X}_{kj} U_{k,j})^{-1/2}, \\
1 - 2\lambda_{kj} &= \alpha_{kj} \beta_{k-1,j} U_{kj}^\top \mathbf{X}_{kj}^\top \mathbf{Y}_{kj} V_{k-1,j} = \rho_n(\mathcal{U}_{kj}, \mathcal{V}_{k-1,j}), \\
V_{kj} &= \mathbf{Y}_{kj}^\dagger \mathbf{X}_{kj} U_{kj} / \|\mathbf{Y}_{kj}^\dagger \mathbf{X}_{kj} U_{kj}\|, \\
\beta_{kj} &= (V_{k,j}^\top \mathbf{Y}_{kj}^\top \mathbf{Y}_{kj} V_{k,j})^{-1/2}, \\
1 - 2\mu_{kj} &= \alpha_{kj} \beta_{kj} U_{kj}^\top \mathbf{X}_{kj}^\top \mathbf{Y}_{kj} V_{k,j} = \rho_n(\mathcal{U}_{kj}, \mathcal{V}_{kj}).
\end{aligned} \tag{13}$$

it is not hard to see that ALS satisfy the stationary condition

$$\begin{aligned}
\nabla_{\alpha, U_j, \lambda} \tilde{\mathcal{L}}(\alpha_{kj}, \mathcal{U}_{kj}, \lambda_{kj}, \beta_{k,j}, \mathcal{V}_{k-1,j}, \mu_{k-1,j}) &= 0, \\
\nabla_{\beta, V_j, \mu} \tilde{\mathcal{L}}(\alpha_{kj}, \mathcal{U}_{kj}, \lambda_{kj}, \beta_{kj}, \mathcal{V}_{kj}, \mu_{kj}) &= 0.
\end{aligned}$$

Therefore ALS alternatively produces iterates that satisfy the stationary condition of (11). However, since we introduced the normalization variables α, β , we changed the subproblem to a non-convex problem. In particular, we do not know if ALS increases the correlation in each iteration or not. To answer this, the following proposition shows that HOPM and ALS generate iterates with the same correlation in each iteration based on the fact that correlation is scale invariant. In particular, this shows that ALS increases the correlation each time it solves the TCCA problem in (8). Moreover, the proposition states that the stationary point of HOPM and ALS are equivalent in the sense that the correlations are the same.

Proposition 3. *Let $(U_{kj}, V_{kj}), (A_{kj}, B_{kj})$ be the iterates generated by HOPM and ALS with the same starting values, respectively. Then, it holds that*

$$U_{kj} = \frac{A_{kj}}{\sqrt{A_{kj}^\top (\frac{1}{n} \mathbf{X}_{kj}^\top \mathbf{X}_{kj}) A_{kj}}}, \quad V_{kj} = \frac{B_{kj}}{\sqrt{B_{kj}^\top (\frac{1}{n} \mathbf{Y}_{kj}^\top \mathbf{Y}_{kj}) B_{kj}}},$$

and

$$\rho_n(\mathcal{U}_{kj}, \mathcal{V}_{kj}) = \rho_n(\mathcal{A}_{kj}, \mathcal{B}_{kj}).$$

Moreover, if $(\alpha, A_1, \dots, A_m, \lambda, \beta, B_1, \dots, B_m, \mu)$ is a critical point of the modified loss $\tilde{\mathcal{L}}$ and $\alpha, \beta > 0$, then $(\alpha^{(1/m)}A_1, \dots, \alpha^{(1/m)}A_m, \beta^{(1/m)}, \lambda, B_1, \dots, \beta^{(1/m)}B_m, \mu)$ is a critical point of the original loss \mathcal{L} .

Ma et al. (2015) used a similar idea to develop a faster algorithm for CCA, called AppGrad. The difference is that we establish the relationship between two alternating minimization schemes, while Ma et al. (2015) established the relationship between gradient descent schemes. Notably, they only show that CCA is a fixed point of AppGrad, while we further illustrate that this type of scheme actually finds a stationary point of a modified non-convex loss (11). Thus ALS and AppGrad are nonconvex methods for the CCA problem. ALS is also related to the optimization on matrix manifold (Absil et al., 2008), but the discussion is beyond the scope of this paper.

4.3 Convergence Analysis

We present our main convergence result for ALS. We start by introducing several assumptions under which we prove the convergence result.

Assumption 1. Assume the following conditions hold:

$$0 < \sigma_{l,x} =: \sigma_{\min}\left(\frac{1}{n} \sum_{t=1}^n \text{vec}(\mathcal{X}_t) \text{vec}(\mathcal{X}_t)^\top\right) < \sigma_{\max}\left(\frac{1}{n} \sum_{t=1}^n \text{vec}(\mathcal{X}_t) \text{vec}(\mathcal{X}_t)^\top\right) := \sigma_{u,x} < \infty,$$

$$0 < \sigma_{l,y} =: \sigma_{\min}\left(\frac{1}{n} \sum_{t=1}^n \text{vec}(\mathcal{Y}_t) \text{vec}(\mathcal{Y}_t)^\top\right) < \sigma_{\max}\left(\frac{1}{n} \sum_{t=1}^n \text{vec}(\mathcal{Y}_t) \text{vec}(\mathcal{Y}_t)^\top\right) := \sigma_{u,y} < \infty,$$

$$\rho_n(\mathcal{U}_0, \mathcal{V}_0) > 0.$$

The same conditions appeared in Ma et al. (2015), who studied CCA for vector valued data. Wang et al. (2017) require the smallest eigenvalue to be bounded away from zero, which can always be achieved by adding the regularization term to the covariance matrix, as discussed in the previous section. However, instead of assuming a bound on the largest eigenvalue, they assume that $\max_i \|x_i\|$ and $\max_i \|y_i\|$ are bounded. The third condition easily be satisfied by noting that if $\rho_n(\mathcal{U}_0, \mathcal{V}_0) < 0$, we can flip the signs of the components of \mathcal{U}_0 or \mathcal{V}_0 to obtain $\rho_n(\mathcal{U}_0, \mathcal{V}_0) > 0$.

Finally, we remark that the first two conditions are sufficient for preventing the iterates from converging to zero. See Lemma 7 for details.

Theorem 4. *If Assumption 1 holds, then the dynamic (13) satisfies Conditions (A1), (A2), and (A3). Furthermore, the iterates U_{kj}, V_{kj} generated by ALS converge to a stationary point at the rate that depends on the exponent in the Lojasiewicz gradient inequality in Lemma 1.*

Theorem 4 establishes a local convergence result that does not depend on any explicit model assumptions. We only require the data to be well conditioned. We note that the local convergence result is not trivial. Experiments in Section 6 illustrate that the SVD-based algorithm does not enjoy this property. However, this convergence analysis does not tell us any information about statistical properties of the estimator, which may require further assumptions on the data generating process.

Although this analysis does not give us an exact convergence rate, [Espig et al. \(2015\)](#), [Espig \(2015\)](#), and [Hu and Li \(2018\)](#) indicated that sublinear, linear and superlinear convergence can happen in the problem of rank-one approximation of a tensor. For the canonical correlation analysis with tensor-valued data, however, we conjecture that with a stronger assumption on a data generating process, it may be possible to get linear convergence. This is corroborated by our experiment in Section 6. We further conjecture that as the sample size increases, the probability that the algorithm converges to a global optimum approaches 1, even when the initial point is chosen randomly. We leave these theoretic justifications under a suitable data generating process for future work.

5 Practical considerations

In this section, we first discuss computational issues associated with TCCA. Inexact updating rule and several useful schemes are included. Moreover, our algorithms and analysis are based on the case where only the first pair of canonical variables is identified based on rank-one decomposition. In practice, we often want to identify additional pairs of canonical variables and seek for a higher rank decomposition. Unfortunately, it is a subtle issue to define the proper notion of the higher rank in the tensor setting. Even worse, obtaining more canonical variables may not be possible, since projection restricted to a low-rank tensor space may not be well-defined. To solve this issue,

we investigate a probabilistic model and observe that 2DCCA is solving CCA with an additional low rank constraint. This leads to the development of a practical deflation procedure.

5.1 Efficient Algorithms for Large-scale Data

The major obstacle in applying CCA to large scale data is that many algorithms involve inversion of large matrices, which is computationally and memory intensive. This problem also appears in Algorithm 1. Inspired by the inexact updating of CCA, we first note that that $\tilde{U}_{kj} = (\mathbf{X}_{kj}^\top \mathbf{X}_{kj})^{-1} \mathbf{X}_{kj}^\top \mathbf{Y}_{kj} V_{k-1,j}$ is the solution to the following least squares problem

$$\min_{\tilde{U}} \frac{1}{2n} \|\mathbf{X}_{kj} \tilde{U} - \mathbf{Y}_{kj} V_{k-1,j}\|^2, \quad (14)$$

and similarly for \tilde{V}_{kj} . In the following theorem, we show that it suffices to solve the least squares problems inexactly. As long as we can bound the error of this inexact update, we will obtain sufficiently accurate estimate of canonical variables. More specifically, we show the error accumulates exponentially. See Algorithm 1 for the complete procedure with inexact updating for ALS or HOPM. Theorem 5 allows us to use advanced stochastic optimization methods for least squares problem, e.g., stochastic variance reduced gradient (Johnson and Zhang, 2013; Shalev-Shwartz and Zhang, 2013).

Theorem 5. Denote $\{U_{kj}^*, V_{kj}^*\}$ generated by option I in Algorithm 1 and U_{kj}, V_{kj} generated by option II in Algorithm 1. Under Assumption 1, we have

$$\max\{\|U_{kj} - U_{kj}^*\|, \|V_{kj} - V_{kj}^*\|\} = O(r^{2mk+j} \sqrt{\epsilon}),$$

for some r that depends on $m, \sigma_{u,x}, \sigma_{l,x}, \sigma_{u,y}, \sigma_{l,y}$.

Note that we obtain the same order for the error bound for the inexact updating bounds as in Wang et al. (2016a), who studied the case with $m = 1$.

Several techniques can be used to speed the convergence of inexact updating of ALS. First, we can use warm-start to initialize the least squares solvers by setting initial points as $\tilde{U}_{k-1,j}, \tilde{V}_{k-1,j}$. Due to the local convergence property, after several iterations, the subproblem (14) of TCCA varies slightly with U_{kj} and V_{kj} , i.e. for large enough k

$$\|U_{kj} - U_{k-1,j}\| \approx 0 \approx \|V_{kj} - V_{k-1,j}\|$$

Therefore we may use $\tilde{U}_{k,j-1}$ as an initialization point when minimizing (14). Second, we can regularize the problem by adding the ridge penalty, or equivalently by setting $r_x, r_y > 0$ in Algorithm 1. The ℓ_2 regularization makes the least squares problem guaranteed to be strongly convex and speeds up the optimization process. This type of regularization is necessary when the size of data is smaller than the dimension of parameters for the condition about smallest eigenvalue in Assumption 1 to be satisfied (Ma et al., 2015; Wang et al., 2018). Finally, the shift-and-invert preconditioning method can be also considered, but we leave this for future work.

5.2 (k_1, k_2, \dots, k_m) -TCCA

We develop a general TCCA procedure for extracting more than one canonical component. We can interpret general TCCA as a higher rank approximation of general CCA. That is, we seek to solve the following CCA problem

$$\min_{\mathcal{U}, \mathcal{V} \text{ in a low-rank space}} \frac{1}{n} \sum_{t=1}^n (\langle \mathcal{U}, \mathcal{X}_t \rangle - \langle \mathcal{V}, \mathcal{Y}_t \rangle)^2 \quad \text{s.t.} \quad \frac{1}{n} \sum_{t=1}^n \langle \mathcal{U}, \mathcal{X}_t \rangle^2 = 1 = \frac{1}{n} \sum_{t=1}^n \langle \mathcal{V}, \mathcal{Y}_t \rangle^2, \quad (15)$$

where \mathcal{U}, \mathcal{V} lie in a ‘‘low-rank’’ space. For example, TCCA restricts solutions \mathcal{U}, \mathcal{V} in the space of rank-one tensors. There are many ways to obtain a higher rank tensor factorization, but here we focus on rank- (r_1, r_2, \dots, r_m) approximation (De Lathauwer et al., 2000a), which is particularly related to 2DCCA and TCCA. For simplicity, we now restrict our discussion to (k_1, k_2) -2DCCA. To perform the (k_1, k_2) -2DCCA, Lee and Choi (2007) obtain $\mathbf{L}_x, \mathbf{L}_y$ by computing the k_1 largest generalized eigenvectors of

$$\begin{bmatrix} 0 & \mathbf{S}_{XY}^r \\ \mathbf{S}_{YX}^r & 0 \end{bmatrix} \begin{bmatrix} L_x \\ L_y \end{bmatrix} = \lambda \begin{bmatrix} \mathbf{S}_{XX}^r + R_x \mathbf{I} & 0 \\ 0 & \mathbf{S}_{YY}^r + R_y \mathbf{I} \end{bmatrix} \begin{bmatrix} L_x \\ L_y \end{bmatrix},$$

where $X_t^r = \mathbf{X}_t R_x, Y_t^r = \mathbf{Y}_t R_y$ and $\mathbf{S}_{XX}^r = \frac{1}{n} \sum_{t=1}^n X_t^r X_t^{r\top}, \mathbf{S}_{XY}^r = \frac{1}{n} \sum_{t=1}^n X_t^r Y_t^{r\top} = (\mathbf{S}_{YX}^r)^\top, \mathbf{S}_{YX}^r = \frac{1}{n} \sum_{t=1}^n Y_t^r X_t^{r\top}$, and similarly for $\mathbf{R}_x, \mathbf{R}_y$. We refer to this method as the SVD-based algorithm for (k_1, k_2) -2DCCA. The corresponding extension of HOPM for (k_1, k_2, \dots, k_m) -TCCA is given in Algorithm 2. Here we replace vectors by matrices. Note that we only need to compute the SVD for small matrices $\tilde{\mathbf{U}}_{kj}^\top (\frac{1}{n} \mathbf{X}_{kj}^\top \mathbf{X}_{kj}) \tilde{\mathbf{U}}_{kj}$ and $\tilde{\mathbf{V}}_{kj}^\top (\frac{1}{n} \mathbf{Y}_{kj}^\top \mathbf{Y}_{kj}) \tilde{\mathbf{V}}_{kj}$.

The main concern with the SVD-based algorithm of Lee and Choi (2007), as well as with

Algorithm 2: Higher-order Power Method for (k_1, \dots, k_m) -TCCA

```

1 Input :  $\{\mathcal{X}_t, \mathcal{Y}_t\}_{t=1}^n \in \mathbb{R}^{d_1 \times \dots \times d_m}$ ,  $k_1, \dots, k_m$ 
2 while not converged do
3   for  $j = 1, 2, \dots, m$  do
4      $\mathbf{X}_{kj} = \sum_{t=1}^n (\mathcal{X}_t)_{(j+1)} (\mathbf{U}_{k-1,m} \cdots \otimes \mathbf{U}_{k-1,j+1} \otimes \mathbf{U}_{k,j-1} \otimes \dots \otimes \mathbf{U}_{k,1})$ 
5      $\mathbf{Y}_{kj} = \sum_{t=1}^n (\mathcal{Y}_t)_{(j+1)} (\mathbf{V}_{k-1,m} \cdots \otimes \mathbf{V}_{k-1,j+1} \otimes \mathbf{V}_{k,j-1} \otimes \dots \otimes \mathbf{V}_{k,1})$ 
6     option I (exact updating):  $\tilde{\mathbf{U}}_{kj} = (\mathbf{X}_{kj}^\top \mathbf{X}_{kj})^{-1} \mathbf{X}_{kj}^\top \mathbf{Y}_{kj} \mathbf{V}_{k-1,j}$ 
7     option II (inexact updating):  $\tilde{\mathbf{U}}_{kj}$  is an  $\epsilon$ -suboptimum of
      
$$\min_{\tilde{\mathbf{U}}} \frac{1}{2n} \|\mathbf{X}_{kj} \tilde{\mathbf{U}} - \mathbf{Y}_{kj} \mathbf{V}_{k-1,j}\|_F^2 + \frac{r_x}{2} \|\tilde{\mathbf{U}}\|_F^2$$

      
$$\mathbf{U}_{kj} = \tilde{\mathbf{U}}_j (\tilde{\mathbf{U}}_{kj}^\top (\frac{1}{n} \mathbf{X}_{kj}^\top \mathbf{X}_{kj}) \tilde{\mathbf{U}}_{kj})^{-1/2}$$

8     option I (exact updating):  $\tilde{\mathbf{V}}_{kj} = (\mathbf{Y}_{kj}^\top \mathbf{Y}_{kj})^{-1} \mathbf{Y}_{kj}^\top \mathbf{X}_{kj} \mathbf{U}_{kj}$ 
9     option II (inexact updating):  $\tilde{\mathbf{V}}_{kj}$  is an  $\epsilon$ -suboptimum of
      
$$\min_{\tilde{\mathbf{V}}} \frac{1}{2n} \|\mathbf{X}_{kj} \tilde{\mathbf{U}}_{kj} - \mathbf{Y}_{kj} \tilde{\mathbf{V}}\|_F^2 + \frac{r_y}{2} \|\tilde{\mathbf{V}}\|_F^2$$

10     $\mathbf{V}_{kj} = \tilde{\mathbf{V}}_j (\tilde{\mathbf{V}}_{kj}^\top (\frac{1}{n} \mathbf{Y}_{kj}^\top \mathbf{Y}_{kj}) \tilde{\mathbf{V}}_{kj})^{-1/2}$ 
    end
11    $k = k + 1$ 
  end
12 Output:  $\mathcal{U}_k, \mathcal{V}_k$ 

```

HOPM, is whether they solve the following (k_1, k_2) -2DCCA problem

$$\begin{aligned}
& \max_{\mathbf{L}_x, \mathbf{R}_x, \mathbf{L}_y, \mathbf{R}_y} \text{Tr} [\text{Cov}((\mathbf{R}_x \otimes \mathbf{L}_x)^\top \text{vec}(\mathbf{X}), (\mathbf{R}_y \otimes \mathbf{L}_y)^\top \text{vec}(\mathbf{Y}))] \\
& \text{s.t.} \quad \mathbb{E} [(\mathbf{R}_x \otimes \mathbf{L}_x)^\top \text{vec}(\mathbf{X}) \text{vec}(\mathbf{X})^\top (\mathbf{R}_x \otimes \mathbf{L}_x)] = \mathbf{I} \\
& \quad \quad \mathbb{E} [(\mathbf{R}_y \otimes \mathbf{L}_y)^\top \text{vec}(\mathbf{Y}) \text{vec}(\mathbf{Y})^\top (\mathbf{R}_y \otimes \mathbf{L}_y)] = \mathbf{I}.
\end{aligned} \tag{16}$$

The answer is no in general, since the iteration sequences of the SVD-based algorithm and HOPM are not feasible. Even worse, (16) may not have a feasible solution due to the fact that the orthogonal relationship in high rank tensor space may not be well-defined, i.e., it may not possible to find \mathbf{U} that satisfies the (k_1, k_2) -2DCCA constraints in general. In what follows, we consider a probabilistic data generating process with a low rank structure. In this setting, we show that it is possible to find a solution to (16) using HOPM. In practice, when the data generating process

is unknown, we can still use HOPM as a non-convex method for low-rank approximation with a relaxation of CCA constraints.

We first introduce the probabilistic model of 2DCCA, which is closely related to factor models appearing in the literature (Virta et al., 2017, 2018; Jendoubi and Strimmer, 2019). Consider two random matrices, $\mathbf{X} \in \mathbb{R}^{m \times n}$, $\mathbf{Y} \in \mathbb{R}^{m \times n}$, distributed according to the following probabilistic model

$$\begin{aligned}\mathbf{X} &= \Phi_1(\mathbf{Z} + \mathbf{E}_x)\Phi_2^\top \\ \mathbf{Y} &= \Omega_1(\mathbf{Z} + \mathbf{E}_y)\Omega_2^\top\end{aligned}\tag{17}$$

where $\mathbf{Z}, \mathbf{E}_x, \mathbf{E}_y$ are random matrices of appropriate dimensions, satisfying $\text{Var}(\text{vec}(\mathbf{Z} + \mathbf{E}_x)) = \mathbf{I} = \text{Var}(\text{vec}(\mathbf{Z} + \mathbf{E}_y))$, and $\Phi_1, \Omega_1 \in \mathbb{R}^{m \times k}$, $\Phi_2, \Omega_2 \in \mathbb{R}^{n \times k}$ are fixed matrices. Note that this probabilistic 2DCCA model is different from the one in Safayani et al. (2018) due to different noise structure. We refer to the 2DCCA model in Safayani et al. (2018) as a 2D-factor model and to our model in (17) as the probabilistic model of 2DCCA or simply, a p2DCCA model.

In practice, the noise structure appearing in the p2DCCA model is more natural than one in the 2D-factor model. Consider the example of image data where X and Y are images of the same object with different illumination conditions. The 2D-factor model implies additive error on images, which is unrealistic. In contrast, the p2DCCA model considers latent variable Z , which corresponds to the common representations, while X and Y are different views obtained from the transformation defined by $\Phi_1, \Phi_2, \Omega_1, \Omega_2$. \mathbf{Z} can represent the magnitude of illumination, the angle of a face, or the gender of a person. The p2DCCA model assumes the error is on the common representation, e.g., the magnitude of illumination. This exactly fits the description of our example and the explanations of latent models. In contrast, the factor model can be better suited for the situations where the additive error is a natural assumption, e.g., time series data (Wang et al., 2019; Chen and Chen, 2017; Chen et al., 2019).

To see how the HOPM solves (16), let $\Phi_1 = \mathbf{M}_1\mathbf{D}_1\mathbf{N}_1^\top$ and $\Phi_2 = \mathbf{M}_2\mathbf{D}_2\mathbf{N}_2^\top$ be the SVDs of Φ_1, Φ_2 . The p2DCCA model implies

$$\begin{aligned}\text{Var}[\text{vec}(\mathbf{X})] &= (\Phi_2\Phi_2^\top) \otimes (\Phi_1\Phi_1^\top) = \mathbf{M}_2\mathbf{D}_2^2\mathbf{M}_2^\top \otimes \mathbf{M}_1\mathbf{D}_1^2\mathbf{M}_1^\top, \\ \frac{1}{n}\mathbb{E}[\mathbf{X}\mathbf{X}^\top] &= \mathbf{M}_1 \text{Tr}(\mathbf{D}_2^2)\mathbf{D}_1^2\mathbf{M}_1^\top := \Sigma_{XX}^1, \\ \frac{1}{m}\mathbb{E}[\mathbf{X}^\top\mathbf{X}] &= \mathbf{M}_2 \text{Tr}(\mathbf{D}_1^2)\mathbf{D}_2^2\mathbf{M}_2^\top := \Sigma_{XX}^2.\end{aligned}\tag{18}$$

Therefore $\text{Var}[\text{vec}((\Sigma_{XX}^1)^{-1/2}\mathbf{X}(\Sigma_{XX}^2)^{-1/2})]$ is a diagonal matrix. Under the p2DCCA model, the mode-wise standardization implies that the elements of $\mathbf{L}_x^\top \mathbf{X} \mathbf{R}_x$ and $\mathbf{L}_y^\top \mathbf{Y} \mathbf{R}_y$ are uncorrelated components, as seen from (18). Therefore, the SVD-based algorithm, as well as HOPM, solves the non-convex extension of CCA exactly.

Note that we can always apply CCA to the data after converting them to vectors. However, this leads to mn -by- mn matrix inversion, while by exploiting the structure in 2DCCA we only need to solve m -by- m and n -by- n matrix inversion instead, which decreases requirement for memory and computation. One drawback of the 2DCC method is that the problem is non-convex and it is possible to get stuck in local optimums even in a noiseless case with $\mathbf{E}_x = 0 = \mathbf{E}_y$. We experimentally verify this phenomena in Section 6.

Without assuming a probabilistic low-rank data generating model, it is not clear whether there is a feasible solution to (16) as discussed above. Here, we discuss a **deflation** procedure that can be used for extracting more than one canonical component (Kruger and Qin, 2003; Sharma et al., 2006). We adapt the method of Kruger and Qin (2003).

Assume the simplest case with $k_1 = 2 = k_2$. Let $\mathbf{U} = (U_1, U_2)$ and $U_1 = U_{11} \otimes U_{12}, U_1 = U_{21} \otimes U_{22}$. In order to see how deflation works, note that for all U_2 satisfy the following equation

$$\frac{1}{n} \sum_t U_1^\top \text{vec}(\hat{\mathcal{X}}_t) \text{vec}(\hat{\mathcal{X}}_t)^\top U_2 = 0,$$

where $\hat{\mathcal{X}}_t = (\mathbf{I} - T_1 T_1^\top) \text{vec}(\mathcal{X}_t)$ is the projected data with $T_1 = (U_1^\top \text{vec}(\mathcal{X}_1), \dots, U_1^\top \text{vec}(\mathcal{X}_n))^\top$. Thus, using the projected idea is similar as uncorrelated constraints in the CCA problem. We can optimize U_1, U_2 in an alternating fashion and similarly for \mathbf{V} . We summarize this procedure in Algorithm 3. Indeed, this is not exactly solving CCA problem but it is a relaxed version of CCA like HOPM for (k_1, \dots, k_m) -TCCA. In practice, even relaxed constraint can improve performance comparing with sample constraint methods such as Partial Least Squares (PLS). See Section 6.2.1 for an application to a genotype data.

5.3 Effective Initialization

In this section, we propose an effective initialization procedure for the $m = 2$ case, focusing on the 2DCCA problem. Since the 2DCCA problem is non-convex, there are no guarantees that ALS converges to a global maximum. Therefore, choosing an initial point is important. We propose to

Algorithm 3: Alternating deflation for TCCA

1 Input : $\mathcal{X}_{1:n}, \mathcal{Y}_{1:n} \in \mathbb{R}^{n \times d_1 \cdots \times d_m}, r$
2 while *not converged* **do**
3 **for** $k = 1, 2, \dots, r$ **do**
4 use $\hat{\mathcal{X}}_k, \hat{\mathcal{Y}}_k$ update $\mathcal{U}_k, \mathcal{V}_k$ by Algorithm 1
5 Compute the residual $\hat{\mathcal{X}}_k = \mathcal{X}_{1:n} \times_1 (\mathbf{I} - T_k T_k^\top), \hat{\mathcal{Y}}_k = \mathcal{Y}_{1:n} \times_1 (\mathbf{I} - S_k S_k^\top)$ where

$$T_k = \begin{bmatrix} \langle \mathcal{U}_1, \mathcal{X}_1 \rangle & \dots & \langle \mathcal{U}_1, \mathcal{X}_n \rangle \\ \vdots & & \vdots \\ \langle \mathcal{U}_{k-1}, \mathcal{X}_1 \rangle & \dots & \langle \mathcal{U}_{k-1}, \mathcal{X}_n \rangle \\ \langle \mathcal{U}_{k+1}, \mathcal{X}_1 \rangle & \dots & \langle \mathcal{U}_{k+1}, \mathcal{X}_n \rangle \\ \vdots & & \vdots \\ \langle \mathcal{U}_r, \mathcal{X}_1 \rangle & \dots & \langle \mathcal{U}_r, \mathcal{X}_n \rangle \end{bmatrix}^\top, S_k = \begin{bmatrix} \langle \mathcal{V}_1, \mathcal{Y}_1 \rangle & \dots & \langle \mathcal{V}_1, \mathcal{Y}_n \rangle \\ \vdots & & \vdots \\ \langle \mathcal{V}_{k-1}, \mathcal{Y}_1 \rangle & \dots & \langle \mathcal{V}_{k-1}, \mathcal{Y}_n \rangle \\ \langle \mathcal{V}_{k+1}, \mathcal{Y}_1 \rangle & \dots & \langle \mathcal{V}_{k+1}, \mathcal{Y}_n \rangle \\ \vdots & & \vdots \\ \langle \mathcal{V}_r, \mathcal{Y}_1 \rangle & \dots & \langle \mathcal{V}_r, \mathcal{Y}_n \rangle \end{bmatrix}^\top$$

end
end
6 Output: $\mathcal{U}_1, \dots, \mathcal{U}_r, \mathcal{V}_1, \dots, \mathcal{V}_r$

initialize the procedure via CCA,

$$(C_x, C_y) = \arg \max_{C_x, C_y} \text{corr}(C_x^\top \text{vec}(\mathcal{X}), C_y^\top \text{vec}(\mathcal{Y})),$$

and use the best rank-1 approximation as the initialization point. More specifically, we find U_1, U_2, V_1, V_2 such that $U_2 \otimes U_1$ and $V_2 \otimes V_1$ are the best approximations of C_x and C_y , which can be obtained by SVD of $\text{unvec}(C_x)$ and $\text{unvec}(C_y)$. Heuristically, an initial point using the best rank-1 approximation may have higher correlation than that of a random guess and, therefore, it is more likely to be close to a global maximum.

Under the p2DCCA model in (17), we showed in last section that the 2DCCA can find the optimum of (16). Under this model, CCA and 2DCCA coincide at the population level. Therefore, as n increases, the CCA solution approaches the global optimum of 2DCCA and it is reasonable to use this as an initialization. We leave the study of the convergence region of a global optimum for future work.

6 Numerical Studies

In this session we carefully examine properties of TCCA through simulation studies and empirical data analysis. We also verify the local convergence property and the effect of the initialization scheme discussed in Section 5.3.

6.1 Simulation

Consider the p2DCCA model of (17) for $t = 1, \dots, n$,

$$\begin{aligned} X_t &= \Phi_1(\Lambda_1 \odot \mathbf{C}_t + \Lambda_2 \odot \mathbf{E}_{xt})\Phi_2^\top, \\ Y_t &= \Omega_1(\Lambda_1 \odot \mathbf{C}_t + \Lambda_2 \odot \mathbf{E}_{yt})\Omega_2^\top, \end{aligned} \quad (19)$$

where \odot denotes the entry-wise (Hadamard) product, $\Phi_1 \in \mathbb{R}^{m_x \times k}$, $\Phi_2 \in \mathbb{R}^{n_x \times k}$, $\Omega_1 \in \mathbb{R}^{m_y \times k}$, $\Omega_2 \in \mathbb{R}^{n_y \times k}$, and $\Phi_1, \Phi_2, \Omega_1, \Omega_2$ are generated randomly to satisfy $\Phi_1^\top \Phi_1 = \mathbf{I} = \Phi_2^\top \Phi_2 = \Omega_1^\top \Omega_1 = \Omega_2^\top \Omega_2$. We achieve this by first generating matrices with elements being random draws from $N(0, 1)$ and then performing the QR decomposition. Λ_i ($i = 1, 2$) are fixed matrices whose elements are between 0 and 1. In the following simulations, we assume the simple case that $k = 2, m_x = 3, n_x = 4, m_y = 4, n_y = 3$ and the elements of $\mathbf{C}_t, \mathbf{E}_{xt}, \mathbf{E}_{yt}$ are random draws from $N(0, 1)$, and

$$\Lambda_1 = \begin{bmatrix} \sqrt{\lambda} & 0 \\ 0 & 0 \end{bmatrix}, \quad \Lambda_2 = \begin{bmatrix} \sqrt{1-\lambda} & 1 \\ 1 & 1 \end{bmatrix}.$$

It is easy to see that in this simple case the two population solutions of CCA and 2DCCA coincide, and the population optimal correlation is λ .

Recall that the 2DCCA aims to find components U_1, U_2, V_1, V_2 solving the following problem:

$$\max_{U_1, U_2, V_1, V_2} \text{Cov}(U_1^\top \mathbf{X}U_2, V_1^\top \mathbf{Y}V_2) \quad \text{s.t.} \quad \text{Var}(U_1^\top \mathbf{X}U_2) = 1 = \text{Var}(V_1^\top \mathbf{Y}V_2).$$

For the first experiment, we generate $n = 100$ samples from (19) with $\lambda = 1$ and apply the HOPM, ALS and SVD-based algorithms 100 times to this data set with 100 random initializations. To test the local convergence property, we check the norm of the difference between consecutive loadings for each iteration k :

$$\text{diff}_k = \|U_{1,k} - U_{1,k-1}\|_2 + \|U_{2,k} - U_{2,k-1}\|_2 + \|V_{1,k} - V_{1,k-1}\|_2 + \|V_{2,k} - V_{2,k-1}\|_2. \quad (20)$$

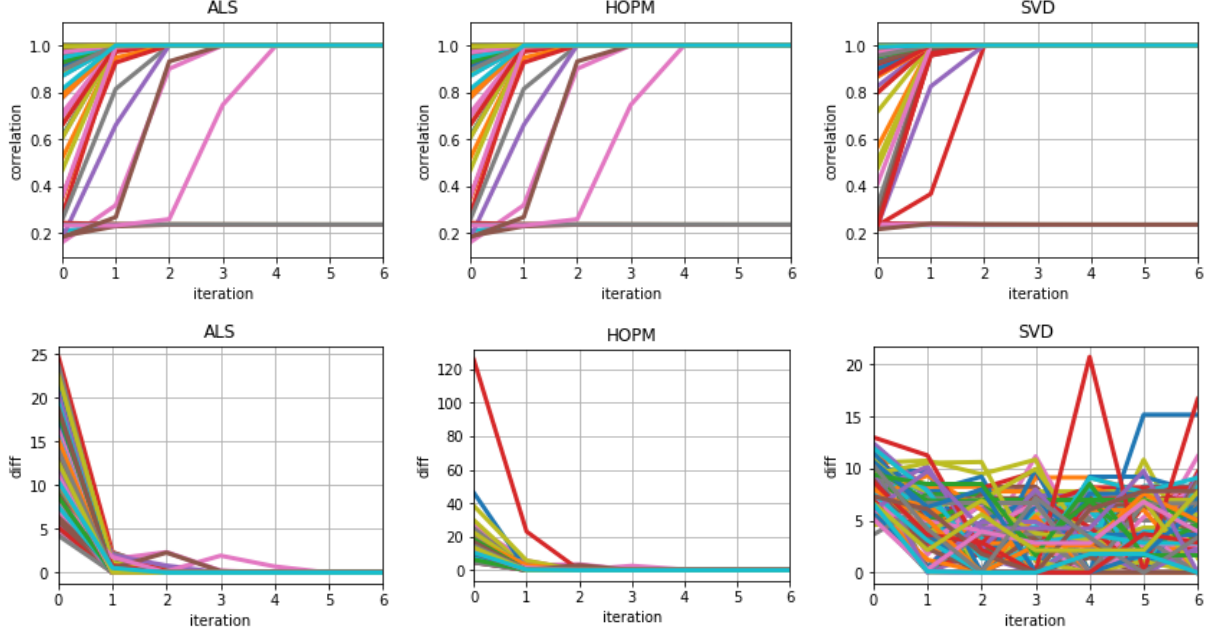


Figure 1: The first row shows the correlation (7) in each iteration, while the second row shows the difference (20) in each iteration. The plots illustrate various methods for 100 random initializations on the same data set. This figure reveals that ALS and HOPM have identical paths of correlation and local convergence property, as explained by our theory. The SVD-based algorithm does not have local convergence property. All methods suffer local optimums even in the noiseless case.

The results are shown in Figure 1. From the plots, we see that the path of correlations of ALS and HOPM are identical and only ALS and HOPM exhibit the local convergence property. The paths of the SVD-based algorithm oscillate due to the unidentifiable property of 2DCCA, which may cause the difficulty of inferring loading coefficient and fail to use the warm start strategy. This phenomenon reveals the non-triviality of our main theorem. Moreover, 5 out of 100 iterations of ALS and 6 out of 100 iterations of SVD-based algorithms fail to achieve the global maximum. Thus, even without any noise, all methods fall in local optimum due to the non-convexity. Note that for each initialization, we run the algorithms for 100 iterations and get the the same results.

Next we study the performance of achieving the global optimum using different sample sizes $n = 50, 100, 300, 700, 1000, 1500$ and different signal-to-noise ratios $\lambda = 0.8, 0.5, 0.2$. Since we do not know the finite-sample closed-form solution of TCCA, we do the following approach to estimate the empirical probabilities of attaining the global maximum, inspired by observing that

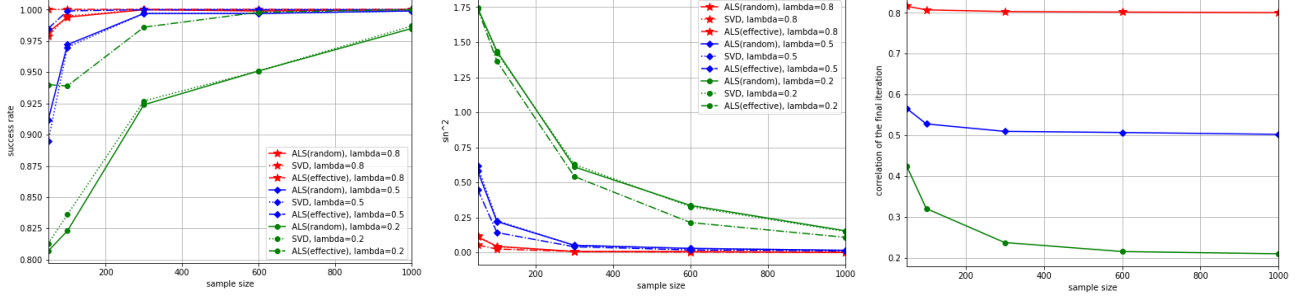


Figure 2: The left figure presents the success rate of achieving global optimum under various conditions obtained by running ALS 15 times in advance with random initialization. The middle figure presents the distance between estimated components and the population solution. The right figure shows the average of correlation of final iteration, which approaches population value. Each point is averaged over 1000 simulation iterations. These figures show that effective initialization improves convergence significantly.

the global maximum is attained by most initializations in Figure 1. We first generate a new dataset each time and run, for a given data set, ALS 15 times with random initialization and treat the resulting maximum correlation as the global maximum. Then, for a given estimation algorithm and a given initialization, we treat the algorithm as a success if the estimated correlation is close to the global maximum of that data set, say, with error $\epsilon = 0.01$. We also compute the distance between the estimated components $\hat{U}_1, \hat{U}_2, \hat{V}_1, \hat{V}_2$ generated by the HOPM, ALS, and SVD-based algorithms and the true population components U_1, U_2, V_1, V_2 , where the error is defined by

$$\text{error} = \text{error}(U_1, \hat{U}_1) + \text{error}(U_2, \hat{U}_2) + \text{error}(V_1, \hat{V}_1) + \text{error}(V_2, \hat{V}_2)$$

with $\text{error}(U_1, \hat{U}_1) = 1 - (U_1^\top \hat{U}_1)^2$. The results are summarized in Figure 2. From the plots, the distance between the estimated and the true population loading goes to 0 when the sample size increases.

The plots also show that with random initialization HOPM and SVD-based algorithms are comparable and an effective initialization not only improves the probability of achieving the global optimum, but also reduces the average distance between the true and sample loadings. Moreover, as the signal-to-noise increases the probability of attaining the global optimum increases and the optimal correlation calculated by running TCCA with 15 different random initializations approaches the population correlation. Finally, our simulation results show that the probability

of achieving the global maximum increases as the sample size increases. This is intuitive and interesting, but we leave a formal theoretical treatment for future research.

6.2 Applications

In this section, we consider three applications of TCCA to demonstrate the power of the proposed analysis in reducing the computational cost and in revealing the data structure.

6.2.1 Gene Expression Data

It is well known that genotype data mirror the population structure (Novembre et al., 2008). Using principal component analysis (PCA), single nucleotide polymorphism (SNP) data of individuals are projected into the first two principal components of the population-genotype matrix and the location information can be recovered. However, this technique cannot be applied to other types of genomics data. In a recent paper, Brown et al. (2018) combined PCA and CCA to overcome this difficulty and reveal certain population structure in gene expression data. The authors notice that the failure of PCA in reconstructing geographical information of the data is caused by the fact that data collected from different laboratories are correlated. They regress the gene expression matrix on data from different laboratories to correct the confounding effect and then perform PCA analysis to extract the first few principal components. Furthermore, they then apply CCA on the batch-corrected expression data and principal components of genotype data to achieve separation of the population in expression data. See Figure 3(a).

Intuitively, principal components of the genotype data are informative in population cluster and can guide the expression data to split the population via CCA. Thus, it is not surprising to see the distinct population patterns in the CCA projection of the expression data. In addition, PCA also serves as a dimensional reduction tool to reduce the computational cost. This is essential because the original genotype data contain around 7 million SNPs.

To exploit the information as much as possible, our goal in this example is to use CCA without the pre-analysis of PCA to achieve similar separation. To this end, we reformulate the expression data and genotype data to matrices and perform TCCA directly. For illustration, we use 318 individuals with genotype data from 1000 genomes phase 1 and corresponding RNA-seq data from GEUVADIS in four populations, GBR, FIN, YRI and TSI, which are the same as those in

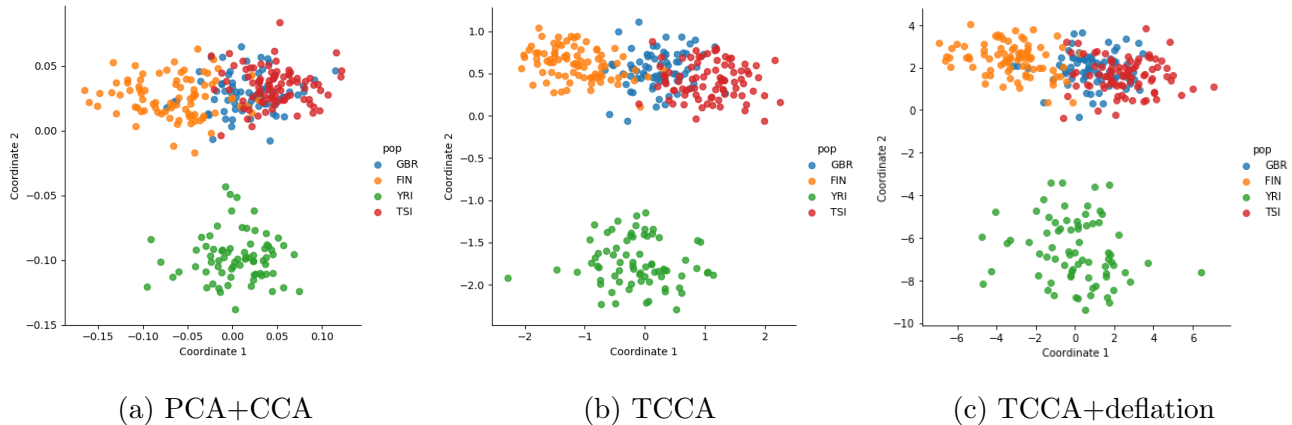


Figure 3: The population structure of gene expression data

[Brown et al. \(2018\)](#) for comparison. We follow the same procedure given in [Brown et al. \(2018\)](#) to extract expression data and remove the confounding. This left 14,079 genes in expression data, which we represent as a 361×39 matrix. The Phase-1 1000 genomes genotypes contain 39,728,178 variants. We use LD pruning, which uses a moving window to compute pairwise correlation and removes highly correlated SNPs. This results in 738,192 SNPs and reformulate them into a 1014×728 matrix. Finally, we perform TCCA and the results are shown in Figure 3(b). The plot clearly shows that TCCA improves the separation. This is encouraging, because our method does not require the selection of the number of PCA components. Moreover, Figure 3(c) shows that TCCA+deflation has a similar improvement.

6.2.2 Air Pollution Data in Taiwan

In this example we use TCCA to analyze air pollution data of Taiwan. The question of interest is whether and how the geographical and meteorological factors affect air pollution. The monthly average data of various air pollution measurements are downloaded from the website of the Environmental Protection Administration, Executive Yuan, Taiwan. We use the data from 2005 to 2017 for a total of 156 months, 12 monitoring stations, and 7 pollutants. The pollutants are sulfur dioxide (SO₂), carbon monoxide (CO), ozone (O₃), particulate matter PM₁₀, oxides of nitrogen (NO_x), nitric oxide (NO), and nitrogen dioxide (NO₂). The measurements of each pollutant in a station are treated as a univariate time series, and we employ a fitted seasonal autoregressive inte-

grated moving-average (ARIMA) model to remove the seasonality. This results in 144 months of seasonally adjusted data for our analysis. Use of seasonally adjusted data is common in economic and environmental studies. The 12 monitoring stations are Guting, Tucheng, Taoyua, Hsinchu, Erlin, Xinying, Xiaogang, Meinong, Yilan, Dongshan, Hualien, and Taitung. See the map in Section B of the Appendix.

To examine the impact of geographical factors, we divide Taiwan into north (Guting, Tucheng, Taoyuan and Hsinchu), south (Erlin, Xinying, Xiaogang and Meinong), and east (Yilan, Dongshan, Hualien and Taitung) regions. There are 4 stations in each region. Again, see Appendix B. Consequently, for this application, we have 144 months by 7 pollutants by 4 stations in each region. We then perform TCCA between regions. To avoid getting trapped in a local maximum, we repeat TCCA 20 times and select the result with the highest correlation as the solution. Tables 1, 2, and 3 summarize the results.

Table 1 shows that the correlations of air pollutants are high between regions, but, as expected, they are not a pure function of the distance between monitoring stations. The eastern stations, on average, are closer to the southern stations than the northern stations, but the correlation between east and south is smaller than that between north and south. This is likely to be caused by the Central Mountain Range in Taiwan with its peaks located in the central and southern parts of Taiwan. Furthermore, the loadings of stations and pollutants shown in Tables 2 and 3 are also informative. The loading coefficients essentially reflect the distances between the stations. The further apart the stations are, the smaller the magnitudes of the loadings. For example, Taitung has a higher loading between South vs East than that between North vs East. A similar effect is also seen in Yilan and Guting. The loadings also reflect the sources of air pollutants. The magnitude of the coefficient of Erlin, which is surrounded by industrial zones and near a thermal power plant, is higher than other stations. The loadings of the pollutants vary, but those of CO are higher and those of PM10 are lower in general.

The wind and rain conditions differ dramatically between summer and winter in Taiwan. In the summer, typhoons and afternoon thunderstorms are common and wind is from the south-east (Pacific Ocean). They reduce the air pollutant concentrations. In contrast, it is dry with strong seasonal wind from the north-west (Mainland) in the winter, leading to higher measurements of pollutant concentrations in winter months. To illustrate these meteorological effects, we divide the

| North vs South | South vs East | North vs East |
|----------------|---------------|---------------|
| 0.888 | 0.817 | 0.904 |

Table 1: The maximum correlations of the data between pairs of regions for Taiwan air pollutants.

| | North | | | | South | | | |
|--------|--------|---------|----------|---------|-------|----------|----------|---------|
| N vs S | Guting | Tucheng | Taoyuan | Hsinchu | Erlin | Xinying | Xiaogang | Meinong |
| | 0.051 | -0.146 | -0.032 | -0.988 | 0.777 | 0.584 | -0.125 | 0.201 |
| | North | | | | East | | | |
| N vs E | Guting | Tucheng | Taoyuan | Hsinchu | Yilan | Dongshan | Hualien | Taitung |
| | 0.627 | 0.671 | 0.215 | 0.331 | 0.895 | -0.051 | 0.441 | 0.044 |
| | South | | | | East | | | |
| S vs E | Erlin | Xinying | Xiaogang | Meinong | Yilan | Dongshan | Hualien | Taitung |
| | 0.625 | 0.142 | 0.596 | 0.483 | 0.511 | -0.145 | 0.303 | 0.791 |

Table 2: The loadings of monitoring stations of the first CCA.

| | SO2 | CO | O3 | PM10 | NOx | NO | NO2 |
|---|--------|--------|--------|--------|--------|--------|--------|
| N | 0.001 | 0.478 | -0.322 | -0.132 | -0.417 | 0.604 | 0.333 |
| S | 0.571 | -0.250 | 0.415 | 0.067 | 0.199 | -0.618 | 0.110 |
| N | -0.779 | 0.567 | 0.170 | 0.165 | -0.051 | 0.112 | -0.014 |
| S | -0.027 | -0.566 | 0.402 | 0.409 | 0.212 | 0.010 | -0.552 |
| S | -0.270 | -0.699 | 0.146 | 0.022 | 0.367 | -0.399 | -0.351 |
| E | -0.187 | -0.292 | 0.434 | 0.080 | 0.219 | -0.029 | -0.798 |

Table 3: The loading of pollutants of the first CCA.

| | North vs South | South vs East | North vs East |
|--------|----------------|---------------|---------------|
| Winter | 0.940 | 0.904 | 0.930 |
| Summer | 0.889 | 0.821 | 0.914 |

Table 4: The correlations between regions by season of Taiwan air pollutants.

| | North | | | | South | | | |
|--------|--------|---------|---------|---------|--------|---------|----------|---------|
| N vs S | Guting | Tucheng | Taoyuan | Hsinchu | Erlin | Xinying | Xiaogang | Meinong |
| Winter | 0.423 | 0.060 | 0.078 | 0.901 | -0.925 | -0.344 | 0.161 | -0.024 |
| Summer | 0.400 | -0.277 | -0.189 | -0.853 | 0.834 | 0.435 | 0.206 | 0.270 |

| | North | | | | South | | | |
|--------|--------|---------|---------|---------|--------|----------|---------|---------|
| N vs E | Guting | Tucheng | Taoyuan | Hsinchu | Yilan | Dongshan | Hualien | Taitung |
| Winter | 0.599 | 0.723 | 0.339 | 0.060 | -0.819 | -0.273 | -0.500 | -0.064 |
| Summer | -0.419 | -0.225 | -0.783 | -0.402 | -0.843 | -0.195 | -0.465 | -0.188 |

| | South | | | | East | | | |
|--------|-------|---------|----------|---------|--------|----------|---------|---------|
| S vs E | Erlin | Xinying | Xiaogang | Meinong | Yilan | Dongshan | Hualien | Taitung |
| Winter | 0.961 | -0.061 | 0.116 | 0.244 | -0.462 | -0.143 | -0.751 | -0.449 |
| Summer | 0.354 | 0.798 | 0.300 | 0.386 | 0.733 | -0.363 | 0.332 | 0.469 |

Table 5: The loading of monitoring stations of the first CCA by season.

data by summer and winter. Specifically, January to March and October to December are winter and April to September are summer. Tables 4, 5, and 6 summarize the results of the analysis. This separation reveals more information. The coefficient of Meinong, for instance, is large in Table 2 due to its location. However, in Table 5, it is significantly different between winter and summer in north stations versus south stations. This is understandable because the north side of Meinong station is blocked by mountains that reduce the wind effect in winter (see Appendix B.)

Table 4 shows that, as expected, the correlations between regions are higher during the winter.

| | SO2 | CO | O3 | PM10 | NOx | NO | NO2 |
|-----------|--------|--------|--------|--------|--------|--------|--------|
| N(Winter) | 0.122 | 0.672 | -0.176 | -0.084 | 0.298 | -0.083 | -0.633 |
| S(Winter) | 0.228 | 0.805 | 0.357 | 0.071 | 0.292 | -0.242 | 0.152 |
| N(Summer) | -0.540 | -0.344 | 0.532 | 0.060 | 0.263 | -0.480 | 0.066 |
| S(Summer) | -0.000 | 0.136 | -0.360 | 0.003 | 0.232 | 0.740 | -0.499 |
| N(Winter) | 0.477 | 0.330 | -0.247 | -0.078 | 0.397 | -0.430 | -0.504 |
| E(Winter) | -0.558 | -0.228 | 0.333 | 0.150 | 0.417 | -0.484 | -0.307 |
| N(Summer) | -0.111 | 0.113 | 0.074 | 0.188 | 0.450 | -0.283 | -0.807 |
| E(Summer) | 0.272 | -0.371 | 0.127 | 0.209 | 0.099 | 0.473 | -0.704 |
| S(Winter) | 0.404 | 0.027 | -0.263 | -0.019 | -0.627 | 0.392 | 0.469 |
| E(Winter) | -0.304 | -0.523 | 0.171 | 0.077 | 0.280 | -0.712 | -0.115 |
| S(Summer) | -0.608 | -0.103 | 0.174 | 0.009 | 0.455 | -0.300 | -0.541 |
| E(Summer) | -0.111 | 0.024 | 0.269 | 0.046 | 0.262 | 0.619 | -0.679 |

Table 6: The loadings of pollutants of the first CCA by season.

It is also interesting to see the differences in loadings of stations between winter and summer in Table 5. For instance, consider South vs East, the loadings of the Eastern stations change sign between winter and summer. This is likely to be caused by the change in wind direction. Finally, loadings of PM10 are smaller than those of other pollutants in Table 6, indicating that PM10 behaves differently from the others.

6.2.3 Electricity Demands in Adelaide

In this example we investigate the relationship between electricity demands in Adelaide, Australia, and temperatures measured at Kent Town from Sunday to Saturday between 7/6/1997 and 3/31/2007. The demands and temperatures are measured every half-hour and we represent the data as two 508 by 48 by 7 tensors. To remove the diurnal patterns in the data, we remove time-wise median from the measurements. Diurnal patterns are common in such data as they are affected by human activities and daily weather. We also consider data for day time (10 am to 3

pm) and evening time (6 pm to 11 pm) only to provide a deeper analysis.

We apply the TCCA to the median-adjusted half-hourly electricity demands and temperatures. Tables 7, 8, 9 and 10 summarize the results. From Table 7, the maximum correlation between electricity demand and temperature is 0.973, which is high. This is not surprising as unusual temperatures (large deviations from median) tend to require use of heating or air conditioning. On the other hand, when we focus on data on day time or evening time, the maximum correlations become smaller, but remain substantial. Table 8 shows that (a), as expected, the loadings are all positive and similar in size for each day when all data are used, but (b) the loadings for the evening change sign between weekday and weekend. This indicates that people in Adelaide, Australia, behave differently in the evenings between weekday and weekend.

Table 9 shows that (a) the loadings in the afternoon (from 2 pm to 4 pm) and evening (from 6 pm to 8 pm) tend to be higher and positive, (b) the loadings during the sleeping time (from 11pm to 3am) are small and negative. This behavior is also understandable because people use less electricity while they are sleeping and the temperature tends to be cooler in the evening.

Acknowledgements

The authors thank Chi-Chun Liu for assistance with processing gene expression data and Su-Yun Huang for comments that greatly improved the manuscript.

| All | Day(10am-3pm) | Evening(6pm-11pm) |
|-------|---------------|-------------------|
| 0.973 | 0.885 | 0.714 |

Table 7: Correlations between electricity demands and temperatures. Half-hourly data from Adelaide and Kent Town, Australia.

| | Monday | Tuesday | Wednesday | Thursday | Friday | Saturday | Sunday |
|--------------------|--------|---------|-----------|----------|--------|----------|--------|
| Whole day | 0.240 | 0.413 | 0.385 | 0.436 | 0.420 | 0.441 | 0.244 |
| Day (10am-3pm) | 0.375 | 0.437 | 0.440 | 0.432 | 0.396 | 0.299 | 0.198 |
| Evening (6pm-11pm) | 0.195 | 0.325 | 0.528 | 0.160 | -0.323 | -0.584 | -0.322 |

Table 8: Loadings of days for the electricity demands and temperature data.

| | | | | | | | |
|--------|--------|--------|--------|--------|--------|--------|--------|
| 0 | 1 | 2 | 3 | | | | |
| -0.080 | -0.076 | -0.104 | -0.104 | -0.061 | -0.021 | 0.021 | 0.067 |
| 4 | 5 | 6 | 7 | | | | |
| 0.099 | 0.121 | 0.12 | 0.075 | -0.002 | -0.086 | -0.129 | -0.144 |
| 8 | 9 | 10 | 11 | | | | |
| -0.155 | -0.156 | -0.151 | -0.125 | -0.064 | 0.002 | 0.066 | 0.116 |
| 12 | 13 | 14 | 15 | | | | |
| 0.145 | 0.174 | 0.179 | 0.177 | 0.206 | 0.238 | 0.262 | 0.284 |
| 16 | 17 | 18 | 19 | | | | |
| 0.281 | 0.227 | 0.121 | -0.054 | -0.231 | -0.237 | -0.214 | -0.206 |
| 20 | 21 | 22 | 23 | | | | |
| -0.135 | -0.071 | -0.058 | -0.069 | -0.080 | -0.055 | -0.004 | -0.062 |

Table 9: Loadings of half-hour interval for the electricity demand and temperature data, time is shown by hours.

| | | | | |
|--------|--------|--------|--------|-------|
| 10 | | 11 | | 12 |
| -0.611 | -0.385 | -0.165 | -0.084 | 0.012 |
| | | 13 | | 14 |
| 0.198 | 0.281 | 0.264 | 0.321 | 0.391 |
| 18 | | 19 | | 20 |
| 0.676 | 0.523 | 0.384 | 0.275 | 0.167 |
| | | 21 | | 22 |
| 0.109 | 0.066 | 0.033 | 0.025 | 0.029 |

Table 10: Loadings of daytime and nighttime, time is shown by hours.

References

- P.-A. Absil, R. Mahony, and B. Andrews. Convergence of the iterates of descent methods for analytic cost functions. *SIAM J. Optim.*, 16(2):531–547, 2005.
- P.-A. Absil, R. Mahony, and R. Sepulchre. *Optimization algorithms on matrix manifolds*. Princeton University Press, Princeton, NJ, 2008. With a foreword by Paul Van Dooren.
- Z. Allen-Zhu and Y. Li. Doubly accelerated methods for faster CCA and generalized eigendecomposition. In D. Precup and Y. W. Teh, editors, *Proceedings of the 34th International Conference on Machine Learning, ICML 2017, Sydney, NSW, Australia, 6-11 August 2017*, volume 70 of *Proceedings of Machine Learning Research*, pages 98–106. PMLR, 2017.
- G. Andrew, R. Arora, J. A. Bilmes, and K. Livescu. Deep canonical correlation analysis. In *Proceedings of the 30th International Conference on Machine Learning, ICML 2013, Atlanta, GA, USA, 16-21 June 2013*, volume 28 of *JMLR Workshop and Conference Proceedings*, pages 1247–1255. JMLR.org, 2013.
- R. Arora, A. Cotter, K. Livescu, and N. Srebro. Stochastic optimization for PCA and PLS. In *50th Annual Allerton Conference on Communication, Control, and Computing, Allerton 2012*,

- Allerton Park & Retreat Center, Monticello, IL, USA, October 1-5, 2012*, pages 861–868. IEEE, 2012.
- R. Arora, T. V. Marinov, P. Mianjy, and N. Srebro. Stochastic approximation for canonical correlation analysis. In I. Guyon, U. V. Luxburg, S. Bengio, H. Wallach, R. Fergus, S. Vishwanathan, and R. Garnett, editors, *Advances in Neural Information Processing Systems 30*, pages 4775–4784. Curran Associates, Inc., 2017.
- F. R. Bach and M. I. Jordan. A Probabilistic Interpretation of Canonical Correlation Analysis. *Dept Statist Univ California Berkeley CA Tech Rep*, 688:1–11, 2006.
- K. Bhatia, A. Pacchiano, N. Flammarion, P. L. Bartlett, and M. I. Jordan. Gen-oja: Simple & efficient algorithm for streaming generalized eigenvector computation. In S. Bengio, H. M. Wallach, H. Larochelle, K. Grauman, N. Cesa-Bianchi, and R. Garnett, editors, *Advances in Neural Information Processing Systems 31: Annual Conference on Neural Information Processing Systems 2018, NeurIPS 2018, 3-8 December 2018, Montréal, Canada.*, pages 7016–7025, 2018.
- J. Bolte, T. P. Nguyen, J. Peypouquet, and B. W. Suter. From error bounds to the complexity of first-order descent methods for convex functions. *Mathematical Programming*, 165(2):471–507, 2017.
- B. C. Brown, N. L. Bray, and L. Pachter. Expression reflects population structure. *PLOS Genetics*, 14(12):e1007841, 2018.
- E. Y. Chen, R. S. Tsay, and R. Chen. Constrained factor models for high-dimensional matrix-variate time series. *Journal of the American Statistical Association*, 0(0):1–37, 2019, [arXiv:https://doi.org/10.1080/01621459.2019.1584899](https://doi.org/10.1080/01621459.2019.1584899).
- E. Y. Chen and R. Chen. Factor Models for High-Dimensional Dynamic Networks: with Application to International Trade Flow Time Series 1981-2015. *arXiv*, pages 1–24, 2017, [arXiv:1710.06325](https://arxiv.org/abs/1710.06325).
- Y. Chen and M. J. Wainwright. Fast low-rank estimation by projected gradient descent: General statistical and algorithmic guarantees. *Technical report*, 2015, [arXiv:1509.03025v1](https://arxiv.org/abs/1509.03025).

- L. De Lathauwer, B. De Moor, and J. Vandewalle. On the best rank-1 and rank- (R_1, R_2, \dots, R_N) approximation of higher-order tensors. *SIAM J. Matrix Anal. Appl.*, 21(4):1324–1342, 2000a.
- L. De Lathauwer, B. De Moor, and J. Vandewalle. A multilinear singular value decomposition. *SIAM J. Matrix Anal. Appl.*, 21(4):1253–1278, 2000b.
- M. Espig. Convergence of Alternating Least Squares Optimisation for Rank-One Approximation to High Order Tensors. *arXiv*, 49(0), 2015, [arXiv:arXiv:1503.05431v1](#).
- M. Espig, W. Hackbusch, and A. Khachatryan. On the Convergence of Alternating Least Squares Optimisation in Tensor Format Representations. *arXiv*, 49(0):1–27, 2015, [arXiv:1506.00062](#).
- X. Fu, K. Huang, M. Hong, N. D. Sidiropoulos, and A. M. So. Scalable and flexible multiview MAX-VAR canonical correlation analysis. *IEEE Trans. Signal Processing*, 65(16):4150–4165, 2017.
- K. Fukumizu, F. R. Bach, and A. Gretton. Statistical consistency of kernel canonical correlation analysis. *J. Mach. Learn. Res.*, 8:361–383, 2007.
- C. Gao, D. Garber, N. Srebro, J. Wang, and W. Wang. Stochastic canonical correlation analysis. *arxiv: 1702.06533*, 2017, [arXiv:1702.06533v1](#).
- R. Ge, C. Jin, S. M. Kakade, P. Netrapalli, and A. Sidford. Efficient algorithms for large-scale generalized eigenvector computation and canonical correlation analysis. In M. Balcan and K. Q. Weinberger, editors, *Proceedings of the 33rd International Conference on Machine Learning, ICML 2016, New York City, NY, USA, June 19-24, 2016*, volume 48 of *JMLR Workshop and Conference Proceedings*, pages 2741–2750. JMLR.org, 2016.
- Y. Guan, M. T. Chu, and D. Chu. Convergence analysis of an SVD-based algorithm for the best rank-1 tensor approximation. *Linear Algebra Appl.*, 555:53–69, 2018.
- A. K. Gupta and D. K. Nagar. *Matrix variate distributions*, volume 104 of *Chapman & Hall/CRC Monographs and Surveys in Pure and Applied Mathematics*. Chapman & Hall/CRC, Boca Raton, FL, 2000.

- B. D. Haeffele, E. Young, and R. Vidal. Structured low-rank matrix factorization: Optimality, algorithm, and applications to image processing. In *Proceedings of the 31th International Conference on Machine Learning, ICML 2014, Beijing, China, 21-26 June 2014*, volume 32 of *JMLR Workshop and Conference Proceedings*, pages 2007–2015. JMLR.org, 2014.
- D. R. Hardoon, S. Szedmák, and J. Shawe-Taylor. Canonical correlation analysis: An overview with application to learning methods. *Neural Computation*, 16(12):2639–2664, 2004.
- H. Hotelling. Relations between two sets of variates. *Biometrika*, 28(3/4):321, 1936.
- S. Hu and G. Li. Convergence rate analysis for the higher order power method in best rank one approximations of tensors. *Numer. Math.*, 140(4):993–1031, 2018.
- T. Jendoubi and K. Strimmer. A whitening approach to probabilistic canonical correlation analysis for omics data integration. *BMC Bioinformatics*, 20(1), 2019.
- C. Jin, W. Mao, R. Zhang, Y. Zhang, and X. Xue. Cross-modal image clustering via canonical correlation analysis. In B. Bonet and S. Koenig, editors, *Proceedings of the Twenty-Ninth AAAI Conference on Artificial Intelligence, January 25-30, 2015, Austin, Texas, USA.*, pages 151–159. AAAI Press, 2015.
- R. Johnson and T. Zhang. Accelerating stochastic gradient descent using predictive variance reduction. In C. J. C. Burges, L. Bottou, M. Welling, Z. Ghahramani, and K. Q. Weinberger, editors, *Advances in Neural Information Processing Systems 26*, pages 315–323. Curran Associates, Inc., 2013.
- D. Kalman. Generalized Fibonacci numbers by matrix methods. *Fibonacci Quart.*, 20(1):73–76, 1982.
- H. Karimi, J. Nutini, and M. W. Schmidt. Linear convergence of gradient and proximal-gradient methods under the polyak-łojasiewicz condition. In P. Frasconi, N. Landwehr, G. Manco, and J. Vreeken, editors, *Machine Learning and Knowledge Discovery in Databases - European Conference, ECML PKDD 2016, Riva del Garda, Italy, September 19-23, 2016, Proceedings, Part I*, volume 9851 of *Lecture Notes in Computer Science*, pages 795–811. Springer, 2016.

- T. Kim, S. Wong, and R. Cipolla. Tensor canonical correlation analysis for action classification. In *2007 IEEE Computer Society Conference on Computer Vision and Pattern Recognition (CVPR 2007)*, 18-23 June 2007, Minneapolis, Minnesota, USA. IEEE Computer Society, 2007.
- T. G. Kolda and B. W. Bader. Tensor decompositions and applications. *SIAM Rev.*, 51(3): 455–500, 2009.
- T. Kollo and D. von Rosen. *Advanced multivariate statistics with matrices*, volume 579 of *Mathematics and Its Applications (New York)*. Springer, Dordrecht, 2005.
- U. Kruger and S. J. Qin. Canonical correlation partial least squares. *IFAC Proceedings Volumes*, 36(16):1603–1608, 2003.
- S. H. Lee and S. Choi. Two-dimensional canonical correlation analysis. *IEEE Signal Processing Letters*, 14(10):735–738, 2007.
- C. Leng and C. Y. Tang. Sparse matrix graphical models. *J. Amer. Statist. Assoc.*, 107(499): 1187–1200, 2012.
- G. Li and T. K. Pong. Calculus of the exponent of Kurdyka-łojasiewicz inequality and its applications to linear convergence of first-order methods. *Found. Comput. Math.*, 18(5):1199–1232, 2018.
- Y. Li, C. Ma, Y. Chen, and Y. Chi. Nonconvex matrix factorization from rank-one measurements. In K. Chaudhuri and M. Sugiyama, editors, *Proceedings of Machine Learning Research*, volume 89 of *Proceedings of Machine Learning Research*, pages 1496–1505. PMLR, 2019.
- Z. Li, A. Uschmajew, and S. Zhang. On convergence of the maximum block improvement method. *SIAM J. Optim.*, 25(1):210–233, 2015.
- H. Liu, A. M.-C. So, and W. Wu. Quadratic optimization with orthogonality constraint: explicit łojasiewicz exponent and linear convergence of retraction-based line-search and stochastic variance-reduced gradient methods. *Mathematical Programming*, 2018.
- S. Łojasiewicz. Ensemble semi-analytique. *Note des cours, Institut des Hautes Etudes Scientifique*, 1965.

- D. Lopez-Paz, S. Sra, A. J. Smola, Z. Ghahramani, and B. Schölkopf. Randomized nonlinear component analysis. In *Proceedings of the 31th International Conference on Machine Learning, ICML 2014, Beijing, China, 21-26 June 2014*, volume 32 of *JMLR Workshop and Conference Proceedings*, pages 1359–1367. JMLR.org, 2014.
- H. Lu, K. N. Plataniotis, and A. N. Venetsanopoulos. A survey of multilinear subspace learning for tensor data. *Pattern Recognition*, 44(7):1540–1551, 2011.
- Y. Luo, D. Tao, K. Ramamohanarao, C. Xu, and Y. Wen. Tensor canonical correlation analysis for multi-view dimension reduction. *IEEE Trans. Knowl. Data Eng.*, 27(11):3111–3124, 2015.
- Z.-Q. Luo and P. Tseng. Error bounds and convergence analysis of feasible descent methods: a general approach. *Annals of Operations Research*, 46(1):157–178, 1993.
- Z. Ma, Y. Lu, and D. P. Foster. Finding linear structure in large datasets with scalable canonical correlation analysis. In F. R. Bach and D. M. Blei, editors, *Proceedings of the 32nd International Conference on Machine Learning, ICML 2015, Lille, France, 6-11 July 2015*, volume 37 of *JMLR Proceedings*, pages 169–178. JMLR.org, 2015.
- A. M. Manceur and P. Dutilleul. Maximum likelihood estimation for the tensor normal distribution: algorithm, minimum sample size, and empirical bias and dispersion. *J. Comput. Appl. Math.*, 239:37–49, 2013.
- T. Michaeli, W. Wang, and K. Livescu. Nonparametric canonical correlation analysis. In M. Balcan and K. Q. Weinberger, editors, *Proceedings of the 33rd International Conference on Machine Learning, ICML 2016, New York City, NY, USA, June 19-24, 2016*, volume 48 of *JMLR Workshop and Conference Proceedings*, pages 1967–1976. JMLR.org, 2016.
- E. P. Miles, Jr. Generalized Fibonacci numbers and associated matrices. *Amer. Math. Monthly*, 67:745–752, 1960.
- Y. Mroueh, E. Marcheret, and V. Goel. Asymmetrically Weighted CCA And Hierarchical Kernel Sentence Embedding For Image and Text Retrieval. *arXiv*, 2016, [arXiv:arXiv:1511.06267v5](https://arxiv.org/abs/1511.06267v5).

- J. Novembre, T. Johnson, K. Bryc, Z. Kutalik, A. R. Boyko, A. Auton, A. Indap, K. S. King, S. Bergmann, M. R. Nelson, M. Stephens, and C. D. Bustamante. Genes mirror geography within europe. *Nature*, 456(7218):98–101, 2008.
- M. Ohlson, M. Rauf Ahmad, and D. von Rosen. The multilinear normal distribution: introduction and some basic properties. *J. Multivariate Anal.*, 113:37–47, 2013.
- D. Park, A. Kyrillidis, C. Caramanis, and S. Sanghavi. Non-square matrix sensing without spurious local minima via the burer-monteiro approach. In A. Singh and X. J. Zhu, editors, *Proceedings of the 20th International Conference on Artificial Intelligence and Statistics, AISTATS 2017, 20-22 April 2017, Fort Lauderdale, FL, USA*, volume 54 of *Proceedings of Machine Learning Research*, pages 65–74. PMLR, 2017.
- D. Park, A. Kyrillidis, C. Caramanis, and S. Sanghavi. Finding low-rank solutions via nonconvex matrix factorization, efficiently and provably. *SIAM J. Imaging Sciences*, 11(4):2165–2204, 2018.
- K. Pearson. On lines and planes of closest fit to systems of points in space. *The London, Edinburgh, and Dublin Philosophical Magazine and Journal of Science*, 2(11):559–572, 1901.
- P. A. Regalia and E. Kofidis. The higher-order power method revisited: convergence proofs and effective initialization. In *IEEE International Conference on Acoustics, Speech, and Signal Processing. ICASSP 2000, 5-9 June, 2000, Hilton Hotel and Convention Center, Istanbul, Turkey*, pages 2709–2712. IEEE, 2000.
- M. Safayani, S. H. Ahmadi, H. Afrabandpey, and A. Mirzaei. An EM based probabilistic two-dimensional CCA with application to face recognition. *Appl. Intell.*, 48(3):755–770, 2018.
- R. Schneider and A. Uschmajew. Convergence results for projected line-search methods on varieties of low-rank matrices via łojasiewicz inequality. *SIAM J. Optim.*, 25(1):622–646, 2015.
- S. Shalev-Shwartz and T. Zhang. Stochastic dual coordinate ascent methods for regularized loss minimization. *J. Mach. Learn. Res.*, 14:567–599, 2013.
- S. K. Sharma, U. Kruger, and G. W. Irwin. Deflation based nonlinear canonical correlation analysis. *Chemometrics and Intelligent Laboratory Systems*, 83(1):34–43, 2006.

- C. Sun and R. Dai. A decomposition method for nonconvex quadratically constrained quadratic programs. In *2017 American Control Conference, ACC 2017, Seattle, WA, USA, May 24-26, 2017*, pages 4631–4636. IEEE, 2017.
- S. Sun. A survey of multi-view machine learning. *Neural Computing and Applications*, 23(7-8): 2031–2038, 2013.
- T. Sun and S. Chen. Class label versus sample label-based CCA. *Applied Mathematics and Computation*, 185(1):272–283, 2007.
- A. Uschmajew. A new convergence proof for the higher-order power method and generalizations. *Pac. J. Optim.*, 11(2):309–321, 2015.
- J. Virta, B. Li, K. Nordhausen, and H. Oja. Independent component analysis for tensor-valued data. *J. Multivariate Anal.*, 162:172–192, 2017.
- J. Virta, B. Li, K. Nordhausen, and H. Oja. JADE for tensor-valued observations. *J. Comput. Graph. Statist.*, 27(3):628–637, 2018.
- D. Wang, X. Liu, and R. Chen. Factor Models for Matrix-Valued High-Dimensional Time Series. *Journal of Econometrics*, 208(1):231–248, 2019, [arXiv:1610.01889](https://arxiv.org/abs/1610.01889).
- J. Wang, M. Kolar, N. Srebro, and T. Zhang. Efficient distributed learning with sparsity. In D. Precup and Y. W. Teh, editors, *Proceedings of the 34th International Conference on Machine Learning*, volume 70 of *Proceedings of Machine Learning Research*, pages 3636–3645, International Convention Centre, Sydney, Australia, 2017. PMLR.
- J. Wang, W. Wang, D. Garber, and N. Srebro. Efficient coordinate-wise leading eigenvector computation. In F. Janoos, M. Mohri, and K. Sridharan, editors, *Algorithmic Learning Theory, ALT 2018, 7-9 April 2018, Lanzarote, Canary Islands, Spain*, volume 83 of *Proceedings of Machine Learning Research*, pages 806–820. PMLR, 2018.
- W. Wang, J. Wang, D. Garber, and N. Srebro. Efficient globally convergent stochastic optimization for canonical correlation analysis. In D. D. Lee, M. Sugiyama, U. V. Luxburg, I. Guyon, and R. Garnett, editors, *Advances in Neural Information Processing Systems 29*, pages 766–774. Curran Associates, Inc., 2016a.

- W. Wang, X. Yan, H. Lee, and K. Livescu. Deep Variational Canonical Correlation Analysis. *arXiv*, 1, 2016b, [arXiv:1610.03454](https://arxiv.org/abs/1610.03454).
- Z. Wen, W. Yin, and Y. Zhang. Solving a low-rank factorization model for matrix completion by a nonlinear successive over-relaxation algorithm. *Math. Program. Comput.*, 4(4):333–361, 2012.
- K. Werner, M. Jansson, and P. Stoica. On estimation of covariance matrices with Kronecker product structure. *IEEE Trans. Signal Process.*, 56(2):478–491, 2008.
- D. A. Wolfram. Solving generalized Fibonacci recurrences. *Fibonacci Quart.*, 36(2):129–145, 1998.
- P. Xu, B. D. He, C. D. Sa, I. Mitliagkas, and C. Ré. Accelerated stochastic power iteration. In A. J. Storkey and F. Pérez-Cruz, editors, *International Conference on Artificial Intelligence and Statistics, AISTATS 2018, 9-11 April 2018, Playa Blanca, Lanzarote, Canary Islands, Spain*, volume 84 of *Proceedings of Machine Learning Research*, pages 58–67. PMLR, 2018.
- Y. Xu and W. Yin. A block coordinate descent method for regularized multiconvex optimization with applications to nonnegative tensor factorization and completion. *SIAM J. Imaging Sci.*, 6(3):1758–1789, 2013.
- J. Yang, D. Zhang, A. F. Frangi, and J.-Y. Yang. Two-dimensional PCA: A new approach to appearance-based face representation and recognition. *IEEE Trans. Pattern Anal. Mach. Intell.*, 26(1):131–137, 2004.
- M. Yang, Q. Sun, and D. Xia. Two-dimensional partial least squares and its application in image recognition. In D. Huang, D. C. W. II, D. S. Levine, and K. Jo, editors, *Advanced Intelligent Computing Theories and Applications. With Aspects of Contemporary Intelligent Computing Techniques, 4th International Conference on Intelligent Computing, ICIC 2008, Shanghai, China, September 15-18, 2008, Proceedings*, volume 15 of *Communications in Computer and Information Science*, pages 208–215. Springer, 2008.
- J. Ye, R. Janardan, and Q. Li. Two-dimensional linear discriminant analysis. In *Advances in Neural Information Processing Systems 17 [Neural Information Processing Systems, NIPS 2004, December 13-18, 2004, Vancouver, British Columbia, Canada]*, pages 1569–1576, 2004.

- F. Yger, M. Berar, G. Gasso, and A. Rakotomamonjy. Adaptive canonical correlation analysis based on matrix manifolds. In *Proceedings of the 29th International Conference on Machine Learning, ICML 2012, Edinburgh, Scotland, UK, June 26 - July 1, 2012*. icml.cc / Omnipress, 2012.
- J. Yin and H. Li. Model selection and estimation in the matrix normal graphical model. *J. Multivariate Anal.*, 107:119–140, 2012.
- M. Yu, V. Gupta, and M. Kolar. An influence-receptivity model for topic based information cascades. In V. Raghavan, S. Aluru, G. Karypis, L. Miele, and X. Wu, editors, *2017 IEEE International Conference on Data Mining, ICDM 2017, New Orleans, LA, USA, November 18-21, 2017*, pages 1141–1146. IEEE Computer Society, 2017.
- M. Yu, Z. Yang, T. Zhao, M. Kolar, and Z. Wang. Provable gaussian embedding with one observation. In S. Bengio, H. M. Wallach, H. Larochelle, K. Grauman, N. Cesa-Bianchi, and R. Garnett, editors, *Advances in Neural Information Processing Systems 31: Annual Conference on Neural Information Processing Systems 2018, NeurIPS 2018, 3-8 December 2018, Montréal, Canada.*, pages 6765–6775, 2018.
- M. Yu, V. Gupta, and M. Kolar. Learning influence-receptivity network structure with guarantee. In K. Chaudhuri and M. Sugiyama, editors, *Proceedings of Machine Learning Research*, volume 89 of *Proceedings of Machine Learning Research*, pages 1476–1485. PMLR, 2019.
- D. Zhang and Z. Zhou. $(2d)^2$ pca: Two-directional two-dimensional PCA for efficient face representation and recognition. *Neurocomputing*, 69(1-3):224–231, 2005.
- J. Zhao and C. Leng. Structured Lasso for regression with matrix covariates. *Statist. Sinica*, 24(2):799–814, 2014.
- T. Zhao, Z. Wang, and H. Liu. A nonconvex optimization framework for low rank matrix estimation. In C. Cortes, N. D. Lawrence, D. D. Lee, M. Sugiyama, and R. Garnett, editors, *Advances in Neural Information Processing Systems 28: Annual Conference on Neural Information Processing Systems 2015, December 7-12, 2015, Montreal, Quebec, Canada*, pages 559–567, 2015.

H. Zhou and L. Li. Regularized matrix regression. *J. R. Stat. Soc. Ser. B. Stat. Methodol.*, 76(2): 463–483, 2014.

A Technical Proofs

A.1 Proof of Proposition 3

Our goal here is to show the connection between HOPM and ALS. It suffices to show that there exist $a_{kj} > 0, b_{kj} > 0$, for all k, j , such that

$$U_{kj} = a_{kj}A_{kj}, \quad V_{kj} = b_{kj}B_{kj}.$$

We show this by induction. Since both algorithms start at the same point, the result holds for $k = 0, j = 1, \dots, m$. By the hypothesis and construction of A_{kj} , we have

$$\begin{aligned} U_{kj} &= \frac{\mathbf{X}_{kj}^\dagger \mathbf{Y}_{kj} V_{k-1,j}}{\sqrt{V_{k-1,j}^\top \mathbf{Y}_{kj}^\top \mathbf{X}_{kj} \mathbf{X}_{kj}^\dagger \mathbf{Y}_{kj} V_{k-1,j}}} \\ &= \frac{b_{kj} \mathbf{X}_{kj}^\dagger \mathbf{Y}_{kj} B_{k-1,j}}{\sqrt{V_{k-1,j}^\top \mathbf{Y}_{kj}^\top \mathbf{X}_{kj} \mathbf{X}_{kj}^\dagger \mathbf{Y}_{kj} V_{k-1,j}}} \\ &= \frac{b_{kj} \|\mathbf{X}_{kj}^\dagger \mathbf{Y}_{kj} B_{k-1,j}\| A_{kj}}{\sqrt{V_{k-1,j}^\top \mathbf{Y}_{kj}^\top \mathbf{X}_{kj} \mathbf{X}_{kj}^\dagger \mathbf{Y}_{kj} V_{k-1,j}}}. \end{aligned}$$

Similar argument holds for V_{kj} . Because all constants are positive and correlation is scale-invariant, this yields the result. Furthermore, by construction, we have

$$1 = U_{kj}^\top \mathbf{X}_{kj}^\top \mathbf{X}_{kj} U_{kj} = a_{kj}^2 A_{kj}^\top \mathbf{X}_{kj}^\top \mathbf{X}_{kj} A_{kj}.$$

Following the same argument for $V_{kj} = B_{kj} / \sqrt{B_{kj}^\top (\frac{1}{n} \mathbf{Y}_{kj}^\top \mathbf{Y}_{kj}) B_{kj}}$, we complete the proof of the first claim.

For the second part, we have

$$\begin{aligned} &\alpha^{(1/m)} \nabla_{U_j} \mathcal{L}(\alpha^{(1/m)} A_1, \dots, \alpha^{(1/m)} A_m, \beta^{(1/m)} \lambda, B_1, \dots, \beta^{(1/m)} B_m, \mu) \\ &= \frac{\alpha^2(1-2\lambda)}{n} \mathbf{X}_j^\top \mathbf{X}_j A_j - \frac{\alpha\beta}{n} \mathbf{X}_j^\top \mathbf{Y}_j B_j \\ &= \nabla_{U_j} \tilde{\mathcal{L}}(\alpha, A_1, \dots, A_m, \lambda, \beta, B_1, \dots, B_m, \mu) \\ &= 0, \end{aligned}$$

and

$$\begin{aligned}
& \nabla_{\lambda} \mathcal{L}(\alpha^{(1/m)} A_1, \dots, \alpha^{(1/m)} A_m, \beta^{(1/m)} \lambda, B_1, \dots, \beta^{(1/m)} B_m, \mu) \\
&= 1 - \frac{\alpha^2(1-2\lambda)}{n} \mathbf{X}_j^{\top} \mathbf{X}_j A_j \\
&= \nabla_{\lambda} \tilde{\mathcal{L}}(\alpha, A_1, \dots, A_m, \lambda, \beta, B_1, \dots, B_m, \mu) \\
&= 0.
\end{aligned}$$

Since $\alpha^{(1/m)} > 0$, $\nabla_{U_j} \mathcal{L}(\alpha^{(1/m)} A_1, \dots, \alpha^{(1/m)} A_m, \beta^{(1/m)} \lambda, B_1, \dots, \beta^{(1/m)} B_m, \mu) = 0$. Applying the same argument for $\nabla_{\beta} \mathcal{L}$ and $\nabla_{\mu} \mathcal{L}$, we obtain the proposition.

A.2 Proof of Theorem 4

We need the following technical lemma.

Lemma 6. *Under Assumption 1, we have, for all j, k :*

1. $U_{kj}^{\top} (\frac{1}{n} \mathbf{X}_{kj}^{\top} \mathbf{X}_{kj}) U_{kj} \in [\sigma_{l,x}, \sigma_{u,x}]$.
2. $\alpha_{kj} \in [\sigma_{u,x}^{-1/2}, \sigma_{l,x}^{-1/2}]$.
3. $1 > \lambda_{k+1,j} - \lambda_{k,j} = [(1 - 2\lambda_{k,j}) - (1 - 2\lambda_{k+1,j})]/2 > 0$ and, thus, $\rho_n(\mathcal{U}_{kj}, \mathcal{V}_{kj})$ converges.
4. There exists $\sigma_0 > 0$, independent of k, j , such that

$$\begin{aligned}
& \tilde{\mathcal{L}}(\alpha_{kj}, \mathcal{U}_{k+1,j-1}, \lambda_{k,j}, \beta_{k+1,j-1}, \mathcal{V}_{k+1,j-1}, \mu_{k+1,j-1}) \\
& \quad - \tilde{\mathcal{L}}(\alpha_{k+1,j}, \mathcal{U}_{k+1,j}, \lambda_{k+1,j}, \beta_{k+1,j-1}, \mathcal{V}_{k+1,j-1}, \mu_{k+1,j-1}) \\
& \quad \geq \frac{\sigma_0}{2} [(\alpha_{k+1,j} - \alpha_{k+1,j+1})^2 + \|U_{kj} - U_{k+1,j}\|^2 + (\lambda_{k+1,j} - \lambda_{k+1,j+1})^2].
\end{aligned}$$

Proof. We only prove the case for $m = 2$. Extension to an arbitrary m is straightforward. The first statement follows from the following two identities

$$U_{kj}^{\top} (\frac{1}{n} \mathbf{X}_{kj}^{\top} \mathbf{X}_{kj}) U_{kj} = (U_{k2} \otimes U_{k1})^{\top} (\frac{1}{n} \sum_{t=1}^n \text{vec}(\mathcal{X}_t) \text{vec}(\mathcal{X}_t)^{\top}) (U_{k2} \otimes U_{k1})$$

and

$$(U_{k2} \otimes U_{k1})^{\top} (U_{k2} \otimes U_{k1}) = (U_{k2}^{\top} U_{k2} \otimes U_{k1}^{\top} U_{k1}) = \|U_{k2}\|^2 \|U_{k1}\|^2 = 1.$$

The second statement follows from the definition of α and the first statement.

For statement 3, by Proposition 3, ALS and HOPM have the same correlation in each iteration. Therefore, since HOPM solves the subproblem where all except one component are fixed, the correlation $\rho_n(\mathcal{U}_{kj}, \mathcal{V}_{kj})$ is increasing at every update and the first statement follows by the assumption. Note that $(\alpha_{kj}, \mathcal{U}_{kj})$ is feasible, i.e.,

$$\frac{\alpha_{kj}^2}{n} U_{kj}^\top \mathbf{X}_{k,j}^\top \mathbf{X}_{k,j} U_{kj} = 1 = \frac{\alpha_{k+1,j}^2}{n} U_{k+1,j}^\top \mathbf{X}_{k,j}^\top \mathbf{X}_{k,j} U_{k+1,j},$$

and so

$$\begin{aligned} & \frac{1}{2} \left[\tilde{\mathcal{L}}(\alpha_{kj}, \mathcal{U}_{k+1,j-1}, \lambda_{k,j}, \beta_{k+1,j-1}, \mathcal{V}_{k+1,j-1}, \mu_{k+1,j-1}) \right. \\ & \quad \left. - \tilde{\mathcal{L}}(\alpha_{k+1,j}, \mathcal{U}_{k+1,j}, \lambda_{k+1,j}, \beta_{k+1,j-1}, \mathcal{V}_{k+1,j-1}, \mu_{k+1,j-1}) \right] \\ &= \frac{1}{2} \left[\frac{\alpha_{kj} \beta_{k,j-1}}{n} U_{kj}^\top \mathbf{X}_{k,j}^\top \mathbf{Y}_{kj} V_{k,j-1} - \frac{\alpha_{k+1,j} \beta_{k,j-1}}{n} U_{k+1,j}^\top \mathbf{X}_{k,j}^\top \mathbf{Y}_{kj} V_{k,j-1} \right] \\ &= \frac{1}{2} [(1 - 2\lambda_{kj}) - (1 - 2\lambda_{k+1,j})] \\ &\geq \lambda_{k+1,j} - \lambda_{kj} \\ &\geq (\lambda_{k+1,j} - \lambda_{kj})^2, \end{aligned} \tag{21}$$

where the last inequality holds because $1 > \lambda_{k+1,j} - \lambda_{kj} > 0$. Furthermore, we have

$$\begin{aligned} & \tilde{\mathcal{L}}(\alpha_{kj}, \mathcal{U}_{k+1,j-1}, \lambda_{k,j}, \beta_{k+1,j-1}, \mathcal{V}_{k+1,j-1}, \mu_{k+1,j-1}) \\ & \quad - \tilde{\mathcal{L}}(\alpha_{k+1,j}, \mathcal{U}_{k+1,j}, \lambda_{k+1,j}, \beta_{k+1,j-1}, \mathcal{V}_{k+1,j-1}, \mu_{k+1,j-1}) \\ &= \tilde{\mathcal{L}}(\alpha_{kj}, \mathcal{U}_{k+1,j-1}, \lambda_{k+1,j}, \beta_{k+1,j-1}, \mathcal{V}_{k+1,j-1}, \mu_{k+1,j-1}) \\ & \quad - \tilde{\mathcal{L}}(\alpha_{k+1,j}, \mathcal{U}_{k+1,j}, \lambda_{k+1,j}, \beta_{k+1,j-1}, \mathcal{V}_{k+1,j-1}, \mu_{k+1,j-1}) \\ &= \tilde{\mathcal{L}}(\alpha_{kj}, \mathcal{U}_{k+1,j-1}, \lambda_{k+1,j}, \beta_{k+1,j-1}, \mathcal{V}_{k+1,j-1}, \mu_{k+1,j-1}) \\ & \quad - \tilde{\mathcal{L}}(\alpha_{kj}, \mathcal{U}_{k+1,j}, \lambda_{k+1,j}, \beta_{k+1,j-1}, \mathcal{V}_{k+1,j-1}, \mu_{k+1,j-1}) \\ & \quad + \tilde{\mathcal{L}}(\alpha_{k,j}, \mathcal{U}_{k+1,j}, \lambda_{k+1,j}, \beta_{k+1,j-1}, \mathcal{V}_{k+1,j-1}, \mu_{k+1,j-1}) \\ & \quad - \tilde{\mathcal{L}}(\alpha_{k+1,j}, \mathcal{U}_{k+1,j}, \lambda_{k+1,j}, \beta_{k+1,j-1}, \mathcal{V}_{k+1,j-1}, \mu_{k+1,j-1}). \end{aligned} \tag{22}$$

From the statement 3, we have

$$\begin{aligned} \nabla_\alpha \tilde{\mathcal{L}}(\alpha_{k+1}, \mathcal{U}_{k+1,j}, \lambda_{k+1,j}, \beta_{k+1,j-1}, \mathcal{V}_{k+1,j-1}, \mu_{k+1,j-1}) &= 0, \\ \nabla_\alpha^2 \tilde{\mathcal{L}}(\alpha_{k+1}, \mathcal{U}_{k+1,j}, \lambda_{k+1,j}, \beta_{k+1,j-1}, \mathcal{V}_{k+1,j-1}, \mu_{k+1,j-1}) &= (1 - 2\lambda_{k+1,j}) U_{k+1,j}^\top \left(\frac{1}{n} \mathbf{X}_{k,j}^\top \mathbf{X}_{k,j} \right) U_{k+1,j} > 0, \end{aligned}$$

which implies

$$\begin{aligned}
& \tilde{\mathcal{L}}(\alpha_{k,j}, \mathcal{U}_{k+1,j}, \lambda_{k+1,j}, \beta_{k+1,j-1}, \mathcal{V}_{k+1,j-1}, \mu_{k+1,j-1}) \\
& \quad - \tilde{\mathcal{L}}(\alpha_{k+1,j}, \mathcal{U}_{k+1,j}, \lambda_{k+1,j}, \beta_{k+1,j-1}, \mathcal{V}_{k+1,j-1}, \mu_{k+1,j-1}) \\
& \qquad \qquad \qquad \geq (1 - 2\lambda_{0,0})\sigma_{l,x}(\alpha_{k,j} - \alpha_{k+1,j})^2. \quad (23)
\end{aligned}$$

Also,

$$\begin{aligned}
& \tilde{\mathcal{L}}(\alpha_{k,j}, \mathcal{U}_{k+1,j-1}, \lambda_{k+1,j}, \beta_{k+1,j-1}, \mathcal{V}_{k+1,j-1}, \mu_{k+1,j-1}) \\
& \quad - \tilde{\mathcal{L}}(\alpha_{k,j}, \mathcal{U}_{k+1,j}, \lambda_{k+1,j}, \beta_{k+1,j-1}, \mathcal{V}_{k+1,j-1}, \mu_{k+1,j-1}) \\
& = \alpha_{k,j}^2(1 - 2\lambda_{k+1,j})(U_{k+1,j-1} - U_{k+1,j})^\top \left(\frac{1}{n} \mathbf{X}_{k,j}^\top \mathbf{X}_{k,j}\right) (U_{k+1,j-1} - U_{k+1,j}) \quad (24) \\
& \quad - \alpha_{k,j} \beta_{k,j-1} U_{k,j}^\top \left(\frac{1}{n} \mathbf{X}_{k,j}^\top \mathbf{Y}_{k,j}\right) V_{k,j-1} + \alpha_{k,j} \beta_{k,j-1} U_{k+1,j}^\top \left(\frac{1}{n} \mathbf{X}_{k,j}^\top \mathbf{Y}_{k,j}\right) V_{k+1,j-1} \\
& \geq \sigma_{u,x}^{-1}(1 - 2\lambda_{0,0})(U_{k+1,j-1} - U_{k+1,j})^\top \left(\frac{1}{n} \mathbf{X}_{k,j}^\top \mathbf{X}_{k,j}\right) (U_{k+1,j-1} - U_{k+1,j})
\end{aligned}$$

where the last inequality follows by the fact that

$$U_{k+1,j}^\top \left(\frac{1}{n} \mathbf{X}_{k,j}^\top \mathbf{Y}_{k,j}\right) V_{k,j-1} - U_{k,j}^\top \left(\frac{1}{n} \mathbf{X}_{k,j}^\top \mathbf{Y}_{k,j}\right) V_{k,j-1} > 0,$$

which can be shown by the following: Let $f(U) = U^\top \left(\frac{1}{n} \mathbf{X}_{k,j}^\top \mathbf{Y}_{k,j}\right) V_{k,j-1}$ be a linear function w.r.t. U with the gradient $\left(\frac{1}{n} \mathbf{X}_{k,j}^\top \mathbf{Y}_{k,j}\right) V_{k,j-1}$. Since $\tilde{U}_{k+1,j} = \mathbf{X}_{k,j}^\dagger \mathbf{Y}_{k,j} V_{k,j-1}$, $V_{k,j-1}^\top \left(\frac{1}{n} \mathbf{Y}_{k,j}^\top \mathbf{X}_{k,j}\right) \mathbf{X}_{k,j}^\dagger \mathbf{Y}_{k,j} V_{k,j-1} > 0$, and $\|U_{k,j}\| = 1 = \|U_{k+1,j}\|$, by the property of the project gradient descent on the unit ball, $f((U_{k,j} + \epsilon U_{k+1,j}) / \|U_{k,j} + \epsilon U_{k+1,j}\|) > f(U_{k,j})$ for all $\epsilon > 0$. Letting $\epsilon \rightarrow \infty$, we obtain the desired result.

Combining (21), (23), (24), Statement 1 and Assumption 1, we complete the lemma. \square

Now we are ready to prove Theorem 4. It is clear that $\tilde{\mathcal{L}}$ is analytic, so it suffices to verify the three conditions in Theorem 2.

Stationary Condition. Since other variables only depend on $U_{k+1,j}$ and $V_{k+1,j}$, it suffices to show that $U_{k,j} = U_{k+1,j}$ and $V_{k,j} = V_{k+1,j}$. By a symmetric argument, we only show the part for $U_{k+1,j}$. Note that $\nabla_{U_j} \tilde{\mathcal{L}}(\alpha_{k,j}, \mathcal{U}_{k+1,j}) = 0$ implies $\alpha_{k,j}(1 - \lambda_{k,j}) \mathbf{X}_{k,j}^\top \mathbf{X}_{k,j} U_{k,j} = \mathbf{X}_{k,j}^\top \mathbf{Y}_{k,j} V_{k-1,j}$, so we have $\tilde{U}_{k+1,j} = \alpha_{k,j}(1 - \lambda_{k,j}) U_{k,j}$. After normalization, we obtain $U_{k,j} = U_{k+1,j}$, and the stationary condition follows.

Asymptotic small step-size safeguard. It suffices to show the part for U_{kj} . Since $(1-2\lambda_{k,j}) = \rho_n(\mathcal{U}_{kj}, \mathcal{V}_{kj})$ is bounded and by Statement 2 in Lemma 6, $(\alpha_{kj}, U_{kj}, \lambda_{kj})$ is on a compact set. Combining this fact and

$$\begin{aligned}\nabla_{\alpha, U_j, \lambda} \tilde{\mathcal{L}}(\alpha_{k+1,j}, \mathcal{U}_{k+1,j}, \lambda_{k+1,j}, \beta_{k+1,j-1}, \mathcal{V}_{k+1,j-1}, \mu_{k+1,j-1}) &= 0, \\ \nabla_{\beta, V_j, \mu} \tilde{\mathcal{L}}(\alpha_{k+1,j}, \mathcal{U}_{k+1,j}, \lambda_{k+1,j}, \beta_{k+1,j}, \mathcal{V}_{k+1,j}, \mu_{k+1,j}) &= 0,\end{aligned}$$

we deduce that, for some $L > 0$ independent on k, j ,

$$\begin{aligned}& \|\nabla \tilde{\mathcal{L}}(\alpha_{k0}, \mathcal{U}_{k0}, \lambda_{k0}, \beta_{k0}, \mathcal{V}_{k0}, \mu_{k0})\|^2 \\ &= \sum_j \|\nabla_{U_j} \tilde{\mathcal{L}}(\alpha_{k0}, \mathcal{U}_{k0}, \lambda_{k0}, \beta_{k0}, \mathcal{V}_{k0}, \mu_{k0}) - \nabla_{U_j} \tilde{\mathcal{L}}(\alpha_{k+1,j}, \mathcal{U}_{k+1,j}, \lambda_{k+1,j}, \beta_{k+1,j-1}, \mathcal{V}_{k+1,j-1}, \mu_{k+1,j-1})\|^2 \\ &+ \|\nabla_{\alpha, \lambda} \tilde{\mathcal{L}}(\alpha_{k0}, \mathcal{U}_{k0}, \lambda_{k0}, \beta_{k0}, \mathcal{V}_{k0}, \mu_{k0}) - \nabla_{\alpha, \lambda} \tilde{\mathcal{L}}(\alpha_{km}, \mathcal{U}_{km}, \lambda_{km}, \beta_{k,m-1}, \mathcal{V}_{k,m-1}, \mu_{k,m-1})\|^2 \\ &+ \sum_j \|\nabla_{V_j} \tilde{\mathcal{L}}(\alpha_{k0}, \mathcal{U}_{k0}, \lambda_{k0}, \beta_{k0}, \mathcal{V}_{k0}, \mu_{k0}) - \nabla_{V_j} \tilde{\mathcal{L}}(\alpha_{k+1,j}, \mathcal{U}_{k+1,j}, \lambda_{k+1,j}, \beta_{k+1,j}, \mathcal{V}_{k+1,j}, \mu_{k+1,j})\|^2 \\ &+ \|\nabla_{\beta, \mu} \tilde{\mathcal{L}}(\alpha_{k0}, \mathcal{U}_{k0}, \lambda_{k0}, \beta_{k0}, \mathcal{V}_{k0}, \mu_{k0}) - \nabla_{\beta, \mu} \tilde{\mathcal{L}}(\alpha_{km}, \mathcal{U}_{km}, \lambda_{km}, \beta_{k,m}, \mathcal{V}_{k,m}, \mu_{k,m})\|^2 \\ &\leq L^2(2m+4) \|(\alpha_{k0}, \mathcal{U}_{k0}, \lambda_{k0}, \beta_{k0}, \mathcal{V}_{k0}, \mu_{k0}) - (\alpha_{km}, \mathcal{U}_{km}, \lambda_{km}, \beta_{k,m}, \mathcal{V}_{k,m}, \mu_{k,m})\|^2.\end{aligned}$$

This completes the asymptotic small step-size safeguard condition.

Primary descent condition. We use the fact that updating each component is a least squares problem to prove the following

$$\begin{aligned}& \tilde{\mathcal{L}}(\alpha_{k0}, \mathcal{U}_{k+1,0}, \lambda_{k,0}, \beta_{k+1,0}, \mathcal{V}_{k+1,0}, \mu_{k+1,0}) - \tilde{\mathcal{L}}(\alpha_{k+1,m}, \mathcal{U}_{k+1,m}, \lambda_{k+1,m}, \beta_{k+1,m}, \mathcal{V}_{k+1,m}, \mu_{k+1,m}) \\ &\geq \sum_{j=1}^m \left[\tilde{\mathcal{L}}(\alpha_{k,j-1}, \mathcal{U}_{k+1,j-1}, \lambda_{k,j-1}, \beta_{k,j}, \mathcal{V}_{k+1,j-1}, \mu_{k,j}) - \tilde{\mathcal{L}}(\alpha_{k+1,j}, \mathcal{U}_{k+1,j}, \lambda_{k+1,j}, \beta_{k,j}, \mathcal{V}_{k+1,j-1}, \mu_{k,j}) \right. \\ &\quad \left. + \tilde{\mathcal{L}}(\alpha_{k+1,j}, \mathcal{U}_{k+1,j}, \lambda_{k+1,j}, \beta_{k,j}, \mathcal{V}_{k+1,j-1}, \mu_{k,j}) - \tilde{\mathcal{L}}(\alpha_{k+1,j}, \mathcal{U}_{k+1,j}, \lambda_{k+1,j}, \beta_{k+1,j}, \mathcal{V}_{k+1,j}, \mu_{k+1,j}) \right] \\ &\geq \frac{\sigma_0}{2} \left[\sum_{j=1}^m (\alpha_{k,j} - \alpha_{k+1,j})^2 + (\lambda_{k,j} - \lambda_{k+1,j})^2 + \|U_{k+1,j} - U_{kj}\|^2 \right. \\ &\quad \left. + \sum_{j=1}^m (\beta_{k,j} - \beta_{k+1,j})^2 + (\mu_{k,j} - \mu_{k+1,j})^2 + \|V_{k+1,j} - V_{kj}\|^2 \right] \\ &\geq \frac{\sigma_0}{2} [(\alpha_{k,0} - \alpha_{k+1,m})^2 + (\lambda_{k,0} - \lambda_{k+1,m})^2 + \|\mathcal{U}_{k+1,0} - \mathcal{U}_{k+1,m}\|^2 \\ &\quad + (\beta_{k,0} - \beta_{k+1,m})^2 + (\mu_{k,0} - \mu_{k+1,m})^2 + \|\mathcal{V}_{k+1,j} - \mathcal{V}_{kj}\|^2],\end{aligned}$$

where the last inequality from the triangle inequality. Combining this and the asymptotic small step-size safeguard yields the primary descent condition.

A.3 Proof of Theorem 5

The following lemma establishes the fact that the updating variables never go to zero.

Lemma 7. *Under Assumption 1, for all k, j , we have*

$$\|U_{kj}\| > \sigma_{u,x}^{-1} \sigma_{l,x}^{1/2} \sigma_{l,y}^{1/2} \quad \text{and} \quad \|V_{kj}\| > \sigma_{u,y}^{-1} \sigma_{l,y}^{1/2} \sigma_{l,x}^{1/2}.$$

Proof. We only show the first statement. It is easy to see that

$$\begin{aligned} \|U_{kj}\| &= \|(\mathbf{X}_{kj}^\top \mathbf{X}_{kj})^{-1} \mathbf{X}_{kj} \mathbf{Y}_{kj} V_{k,j-1}\| \\ &\geq \sigma_{u,x} \sigma_{l,x}^{1/2} \sigma_{l,y}^{1/2}, \end{aligned}$$

where the last inequality holds because, for any unit vector U , we have

$$U^\top \mathbf{X}_{kj}^\top \mathbf{X}_{kj} U = (U_{km} \otimes \cdots \otimes U \otimes \cdots \otimes U_{k1})^\top \frac{1}{n} \sum_{t=1}^n \text{vec}(\mathcal{X}_t) \text{vec}(\mathcal{X}_t)^\top (U_{km} \otimes \cdots \otimes U \otimes \cdots \otimes U_{k1}).$$

This complete the proof. \square

With this we show the error bound of inexact updating. We only focus on the U_{kj} since a similar argument directly applies to V_{kj} .

In this proof, we distinguish the iterates of inexact updating power iterations (inexact updating in Algorithm 1) from the iterates of the exact power iterations (exact updating in Algorithm 1) and denote the latter with asterisks, i.e., U_{kj} and U_{kj}^* . Let $f_{kj}(\tilde{U}) = \frac{1}{2n} \|\mathbf{X}_{kj} \tilde{U} - \mathbf{Y}_{kj} V_{k-1,j}\|^2$ and $g_{kj}(\tilde{V}) = \frac{1}{2n} \|\mathbf{X}_{kj} \tilde{U}_{kj} - \mathbf{Y}_{kj} \tilde{V}\|^2$. We denote the exact optimum of $f_{kj}(U)$ and $g_{kj}(V)$ by \tilde{U}_{kj}^\natural and \tilde{V}_{kj}^\natural respectively, and use tilde to indicate that the iterates are unnormalized, i.e., \tilde{U}_{kj} and \tilde{U}_{kj}^* .

We prove the theorem by induction, exploiting the recurrent relationship of the error bound. By the triangle inequality, we have

$$\|U_{kj} - U_{kj}^*\| \leq \|U_{kj} - \tilde{U}_{kj}^\natural\| + \|\tilde{U}_{kj}^\natural - U_{kj}^*\| = \text{(I)} + \text{(II)}. \quad (25)$$

For the first term, by construction and the fact that \tilde{U}_{kj} is an ϵ -suboptimum of f_{kj} , we have

$$\epsilon \geq f_{kj}(\tilde{U}_{kj}) - f_{kj}(\tilde{U}_{kj}^\natural) = \frac{1}{2} (\tilde{U}_{kj} - \tilde{U}_{kj}^\natural)^\top \mathbf{X}_{kj}^\top \mathbf{X}_{kj} (\tilde{U}_{kj} - \tilde{U}_{kj}^\natural) \geq \sigma_{l,x} \|\tilde{U}_{kj} - \tilde{U}_{kj}^\natural\|^2.$$

For the (I) in (25), Lemma 7 implies that $\|\tilde{U}_{kj}^{\natural}\|$ is uniformly bounded below for all k, j , yielding that for some $c > 0$

$$\|U_{kj} - U_{kj}^{\natural}\| \leq \tan^{-1} \left(\frac{\|\tilde{U}_{kj} - \tilde{U}_{kj}^{\natural}\|}{\|\tilde{U}_{kj}^{\natural}\|} \right) \leq c\sigma_{l,x}^{-1}\sqrt{\epsilon}.$$

For the (II) in (25), again by construction, we have

$$\begin{aligned} \|U_{kj} - U_{kj}^*\| &= \|(\mathbf{X}_{k,j}^{\top} \mathbf{X}_{k,j})^{-1} \mathbf{X}_{k,j}^{\top} \mathbf{Y}_{k,j} V_{k-1,j} - ((\mathbf{X}_{k,j}^*)^{\top} \mathbf{X}_{k,j}^*)^{-1} (\mathbf{X}_{k,j}^*)^{\top} \mathbf{Y}_{k,j}^* V_{k-1,j}^*\| \\ &\leq \|(\mathbf{X}_{k,j}^{\top} \mathbf{X}_{k,j})^{-1} \mathbf{X}_{k,j}^{\top} \mathbf{Y}_{k,j} V_{k-1,j} - (\mathbf{X}_{k,j}^{\top} \mathbf{X}_{k,j})^{-1} \mathbf{X}_{k,j}^{\top} \mathbf{Y}_{k,j} V_{k-1,j}^*\| \\ &\quad + \|(\mathbf{X}_{k,j}^{\top} \mathbf{X}_{k,j})^{-1} \mathbf{X}_{k,j}^{\top} \mathbf{Y}_{k,j} V_{k-1,j}^* - (\mathbf{X}_{k,j}^{\top} \mathbf{X}_{k,j})^{-1} \mathbf{X}_{k,j}^{\top} \mathbf{Y}_{k,j}^* V_{k-1,j}^*\| \\ &\quad + \|(\mathbf{X}_{k,j}^{\top} \mathbf{X}_{k,j})^{-1} \mathbf{X}_{k,j}^{\top} \mathbf{Y}_{k,j}^* V_{k-1,j}^* - (\mathbf{X}_{k,j}^{\top} \mathbf{X}_{k,j})^{-1} (\mathbf{X}_{k,j}^*)^{\top} \mathbf{Y}_{k,j}^* V_{k-1,j}^*\| \\ &\quad + \|(\mathbf{X}_{k,j}^{\top} \mathbf{X}_{k,j})^{-1} (\mathbf{X}_{k,j}^*)^{\top} \mathbf{Y}_{k,j}^* V_{k-1,j}^* - ((\mathbf{X}_{k,j}^*)^{\top} \mathbf{X}_{k,j}^*)^{-1} (\mathbf{X}_{k,j}^*)^{\top} \mathbf{Y}_{k,j}^* V_{k-1,j}^*\|, \end{aligned}$$

where $\mathbf{X}_{k,j}^*$ is the exact version of $\mathbf{X}_{k,j}$. Applying the same technique, we obtain

$$\begin{aligned} \|(\mathbf{X}_{k,j}^{\top} \mathbf{X}_{k,j})^{-1} \mathbf{X}_{k,j}^{\top} \mathbf{Y}_{k,j} V_{k-1,j} - (\mathbf{X}_{k,j}^{\top} \mathbf{X}_{k,j})^{-1} \mathbf{X}_{k,j}^{\top} \mathbf{Y}_{k,j} V_{k-1,j}^*\| \\ \leq \left\| \frac{1}{n} (\mathbf{X}_{k,j}^{\top} \mathbf{X}_{k,j})^{-1} \right\| \left\| \frac{1}{\sqrt{n}} \mathbf{X}_{k,j}^{\top} \right\| \left\| \frac{1}{\sqrt{n}} \mathbf{Y}_{k,j} \right\| \|V_{k-1,j} - V_{k-1,j}^*\| \\ \leq \sigma_{l,x}^{-1} \sigma_{u,x}^{1/2} \sigma_{u,y}^{1/2} \|V_{k-1,j} - V_{k-1,j}^*\| \end{aligned}$$

and

$$\begin{aligned} \|(\mathbf{X}_{k,j}^{\top} \mathbf{X}_{k,j})^{-1} \mathbf{X}_{k,j}^{\top} \mathbf{Y}_{k,j} V_{k-1,j}^* - (\mathbf{X}_{k,j}^{\top} \mathbf{X}_{k,j})^{-1} \mathbf{X}_{k,j}^{\top} \mathbf{Y}_{k,j}^* V_{k-1,j}^*\| \\ \leq \left\| \frac{1}{n} (\mathbf{X}_{k,j}^{\top} \mathbf{X}_{k,j})^{-1} \right\| \left\| \frac{1}{\sqrt{n}} \mathbf{X}_{k,j}^{\top} \right\| \left\| \frac{1}{\sqrt{n}} (\mathbf{Y}_{k,j} - \mathbf{Y}_{k,j}^*) \right\| \\ \leq \sigma_{l,x}^{-1} \sigma_{u,x}^{1/2} \sigma_{u,y}^{1/2} \left(\sum_{i < j} \|V_{k,i} - V_{k,i}^*\| + \sum_{i > j} \|V_{k-1,i} - V_{k-1,i}^*\| \right). \end{aligned}$$

By a similar argument,

$$\begin{aligned} \|(\mathbf{X}_{k,j}^{\top} \mathbf{X}_{k,j})^{-1} \mathbf{X}_{k,j}^{\top} \mathbf{Y}_{k,j}^* V_{k-1,j}^* - (\mathbf{X}_{k,j}^{\top} \mathbf{X}_{k,j})^{-1} (\mathbf{X}_{k,j}^*)^{\top} \mathbf{Y}_{k,j}^* V_{k-1,j}^*\| \\ \leq \sigma_{l,x}^{-1} \sigma_{u,x}^{1/2} \sigma_{u,y}^{1/2} \left(\sum_{i < j} \|U_{k,i} - U_{k,i}^*\| + \sum_{i > j} \|U_{k-1,i} - U_{k-1,i}^*\| \right), \\ \|(\mathbf{X}_{k,j}^{\top} \mathbf{X}_{k,j})^{-1} (\mathbf{X}_{k,j}^*)^{\top} \mathbf{Y}_{k,j}^* V_{k-1,j}^* - ((\mathbf{X}_{k,j}^*)^{\top} \mathbf{X}_{k,j}^*)^{-1} (\mathbf{X}_{k,j}^*)^{\top} \mathbf{Y}_{k,j}^* V_{k-1,j}^*\| \\ \leq \sigma_{l,x}^{-1} \sigma_{u,x}^{1/2} \sigma_{u,y}^{1/2} \left(\sum_{i < j} \|U_{k,i} - U_{k,i}^*\| + \sum_{i > j} \|U_{k-1,i} - U_{k-1,i}^*\| \right). \end{aligned}$$

By induction of hypothesis, we have, for some $c > 0$ (the constant may change from line to line)

$$\begin{aligned} \|U_{kj} - U_{kj}^*\| \leq c\sigma_{l,x}^{-1}\sqrt{\epsilon} + 2\sigma_{l,x}^{-1}\sigma_{u,x}^{1/2}\sigma_{u,y}^{1/2} & \left(\sum_{i<j} \|U_{k,i} - U_{ki}^*\| + \sum_{i>j} \|U_{k-1,i} - U_{k-1,i}^*\| \right. \\ & \left. + \sum_{i<j} \|V_{k,i} - V_{ki}^*\| + \sum_{i>j} \|V_{k-1,i} - V_{k-1,i}^*\| \right). \end{aligned}$$

Similarly, we have

$$\begin{aligned} \|V_{kj} - V_{kj}^*\| \leq c\sigma_{l,y}^{-1}\sqrt{\epsilon} + 2\sigma_{l,y}^{-1}\sigma_{u,y}^{1/2}\sigma_{u,x}^{1/2} & \left(\sum_{i<j} \|V_{k,i} - V_{ki}^*\| + \sum_{i>j} \|V_{k-1,i} - V_{k-1,i}^*\| \right. \\ & \left. + \sum_{i<j} \|U_{k,i} - U_{ki}^*\| + \sum_{i>j} \|U_{k-1,i} - U_{k-1,i}^*\| \right). \end{aligned}$$

Define $c_1 = \max\{c\sigma_{l,y}^{-1}, c\sigma_{l,x}^{-1}\}$, $c_2 = \max\{2\sigma_{l,y}^{-1}\sigma_{u,y}^{1/2}\sigma_{u,x}^{1/2}, 2\sigma_{l,x}^{-1}\sigma_{u,x}^{1/2}\sigma_{u,y}^{1/2}\}$,

$$E_\ell = \begin{cases} 0 & \text{if } \ell \leq 0, \\ \|U_{kj} - U_{kj}^*\| & \text{if } \ell > 0 \text{ is odd and } \frac{\ell+1}{2} \bmod 2 = j, \\ \|V_{kj} - V_{kj}^*\| & \text{if } \ell > 0 \text{ is even and } \frac{\ell}{2} \bmod 2 = j, \end{cases}$$

and the $2m$ -th generalized Fibonacci number

$$F_\ell = \begin{cases} 0 & \text{if } \ell \leq 1, \\ c_1\sqrt{\epsilon} & \text{if } \ell = 1, \\ c_2(F_{\ell-1} + F_{\ell-2} + \cdots + F_{\ell-2m}) & \text{if } \ell > 1. \end{cases}$$

Then we have

$$\begin{aligned} E_\ell & \leq c_1\sqrt{\epsilon} + c_2(E_{\ell-1} + E_{\ell-2} + \cdots + E_{\ell-2m}) \\ & = (\ell - 1)c_1\sqrt{\epsilon} + F_\ell. \end{aligned} \tag{26}$$

Following the technique of [Kalman \(1982\)](#) and letting

$$R = \begin{bmatrix} 0 & 1 & 0 & \cdots & 0 & 0 \\ 0 & 0 & 1 & \cdots & 0 & 0 \\ 0 & 0 & 0 & \cdots & 0 & 0 \\ \vdots & \vdots & \vdots & & \vdots & \vdots \\ 0 & 0 & 0 & \cdots & 0 & 1 \\ c_2 & c_2 & c_2 & & c_2 & c_2 \end{bmatrix},$$

we have

$$\begin{bmatrix} F_\ell \\ \vdots \\ F_{\ell+2m-1} \\ F_{\ell+2m} \end{bmatrix} = R^\ell \begin{bmatrix} 0 \\ \vdots \\ 0 \\ c_1\sqrt{\epsilon} \end{bmatrix}.$$

Provided that there are $2m$ distinct eigenvalues of R , denoted r_1, r_2, \dots, r_{2m} , which can be shown as in [Miles \(1960\)](#) and [Wolfram \(1998\)](#), via eigen-decomposition $R = VDV^{-1}$, where

$$V = \begin{bmatrix} 1 & 1 & 1 & \cdots & 1 \\ r_1 & r_2 & r_3 & & r_{2m} \\ r_1^2 & r_2^2 & r_3^2 & \cdots & r_{2m}^2 \\ & & \vdots & & \\ r_1^{2m-1} & r_2^{2m-1} & r_3^{2m-1} & \cdots & r_{2m}^{2m-1} \end{bmatrix},$$

we have

$$\begin{aligned} F_\ell &= [1, 0, \dots, 0]VD^\ell V^{-1} \begin{bmatrix} 0 \\ \vdots \\ 0 \\ c_1\sqrt{\epsilon} \end{bmatrix} \\ &= [r_1^\ell, r_2^\ell, \dots, r_{2m}^\ell]V^{-1} \begin{bmatrix} 0 \\ \vdots \\ 0 \\ c_1 \end{bmatrix} \sqrt{\epsilon} \\ &= \sum_{i=1}^{2m} r_i^\ell z_i \sqrt{\epsilon}, \end{aligned} \tag{27}$$

where z_1, \dots, z_{2m} satisfy

$$V \begin{bmatrix} z_1 \\ \vdots \\ z_{2m-1} \\ z_{2m} \end{bmatrix} = \begin{bmatrix} 0 \\ \vdots \\ 0 \\ c_1 \end{bmatrix}.$$

Combining [\(26\)](#) and [\(27\)](#), we have

$$E_\ell = \left[(\ell - 1)c_1 + \sum_{i=1}^{2m} r_i^\ell z_i \right] \sqrt{\epsilon} = O(r^\ell \sqrt{\epsilon}),$$

where r is the largest eigenvalue of R , which completes the proof.

B Taiwan Map

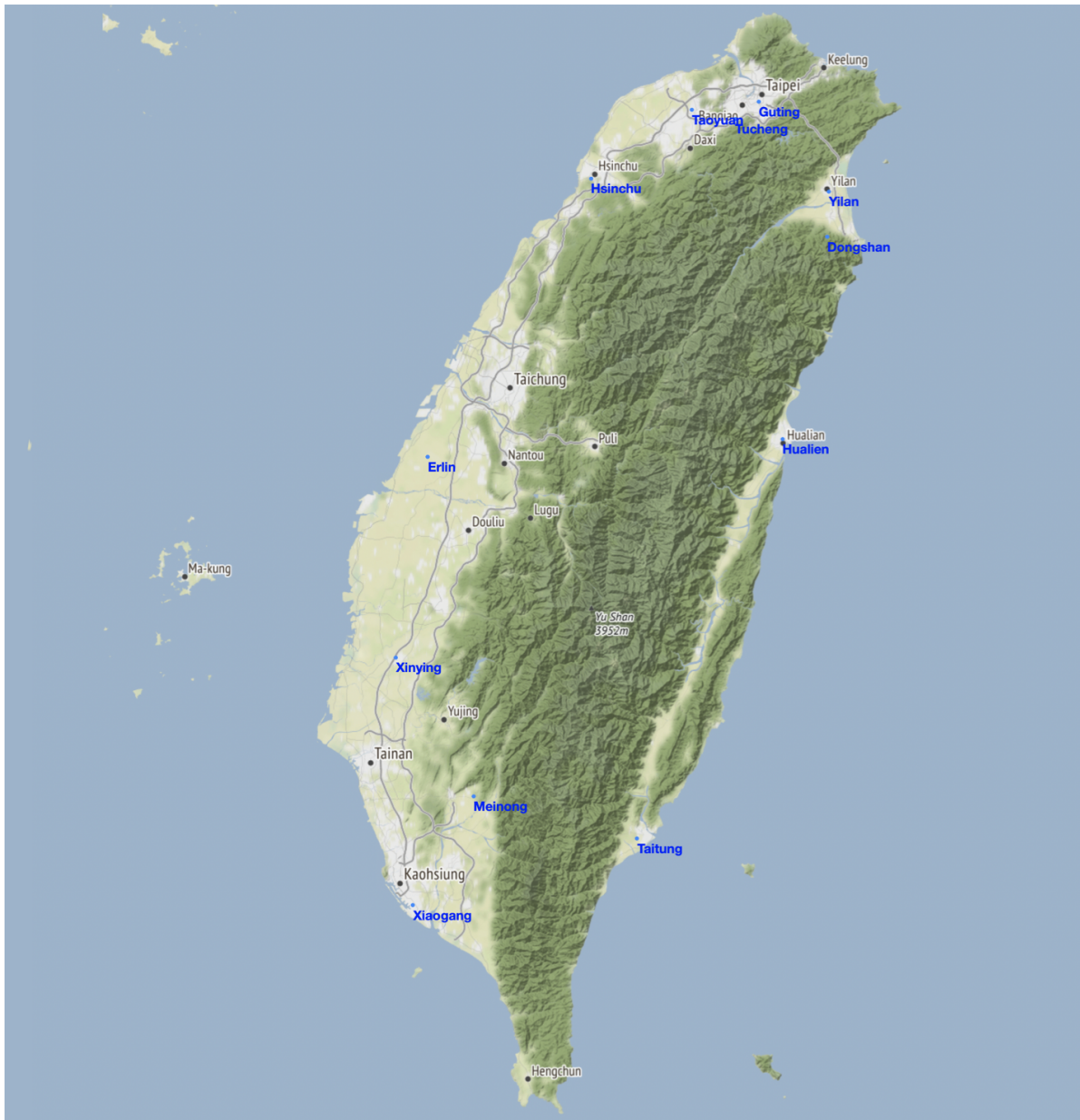


Figure 4: Stations in Taiwan